Journal of Water Process Engineering 66 (2024) 105890

Contents lists available at ScienceDirect

Journal of Water Process Engineering

journal homepage: www.elsevier.com/locate/jwpe

Visible light driven $CuBi_2O_4$ heterostructures and their enhanced photocatalytic activity for pollutant degradation: A review

Olalekan C. Olatunde [a,b,*], Lawrence Sawunyama [a,b], Tunde L. Yusuf [c], Damian C. Onwudiwe [a,b,*]

[a] Materials Science Innovation and Modelling (MaSIM) Research Focus Area, Faculty of Natural and Agricultural Sciences, North-West University, Mafikeng Campus, Private Bag X2046, Mmabatho 2735, South Africa

[b] Department of Chemistry, School of Physical and Chemical Sciences, Faculty of Natural and Agricultural Sciences, North-West University, Mafikeng Campus, Private Bag X2046, Mmabatho 2735, South Africa

[c] Department of Chemistry, Faculty of Natural and Agricultural Sciences, University of Pretoria, Private Bag X20, Hatfield 0028, Pretoria, South Africa

ARTICLE INFO

Editor: Dr Guangming Jiang

Keywords:
$CuBi_2O_4$ heterostructures
Synthetic methods
Mechanism
Photocatalytic degradation

ABSTRACT

The existence of organic, inorganic, and microbiological contaminants in water bodies continues to pose a serious threat to public health worldwide. The photocatalytic elimination of these contaminants using copper bismuthate ($CuBi_2O_4$) heterostructures has been the subject of numerous studies. $CuBi_2O_4$ heterostructures have demonstrated their effectiveness as a photocatalyst because of their longer charge carrier lifespan, enhanced capacity to absorb solar light, and greater charge carrier separation. The various techniques for fabricating $CuBi_2O_4$ heterostructures such as hydrothermal, sol-gel, solid state, solvothermal, electrospinning, spray pyrolysis, and electrodeposition are extensively discussed in this review paper. A wide range of $CuBi_2O_4$ heterostructures and their different mechanisms of action are also covered. The photocatalytic degradation of pollutants by copper bismuthate ($CuBi_2O_4$) heterostructures is also presented in detail. Furthermore, a thorough critical discussion is included about the prospects and difficulties of using $CuBi_2O_4$ heterostructures for the photocatalytic purification of wastewater.

1. Introduction

Global population growth, prolonged droughts, and rapid industrialization have significantly increased the demand for and scarcity of clean water sources [1]. Many practical measures and solutions have been implemented to establish more sustainable water resources in response to this rising demand [2,3]. However, finding sustainable water supplies is increasingly difficult in arid regions with abundant sunshine, minimal precipitation, and extended droughts. Currently, an estimated 4 billion people worldwide lack or have limited access to clean, sanitized water, and millions die each year from severe waterborne illnesses. These statistics are expected to worsen due to rising water contamination caused by excessive contaminants and micropollutants entering the natural water cycle [4–6].

Freshwater resources, including lakes, rivers, and groundwater, are contaminated by various organic, inorganic, and microbiological substances such as agricultural chemicals, pharmaceuticals, and personal care products [7–9]. For example, 20 % of dyes used in the textile industries are discharged as wastewater into the environment. With a medial lethal dose (LD_{50}) of $>2 \times 10^3$ mg/kg and being non-biodegradable, their acute toxicity could result in severe ailments in the human body [10,11]. Similarly, Pharmaceuticals, being non-biodegradable, pose environmental hazards even at low concentrations, contributing to antibiotic resistance and disrupting endocrine and immune systems. Persistent pharmaceutical waste threatens aquatic life by degrading water quality, which is particularly problematic in water-scarce areas where reuse is common [12]. Consequently, developing innovative, affordable, and highly effective wastewater treatment technologies is crucial to prevent the worsening clean water shortage.

Recycling treated municipal wastewater from treatment plants or on-site rural wastewater for industrial and agricultural purposes is a promising solution [13,14]. This approach can significantly contribute to clean water resources since they constitute one of the largest potential water sources [15]. However, recalcitrant organic and inorganic

* Corresponding authors at: Materials Science Innovation and Modelling (MaSIM) Research Focus Area, Faculty of Natural and Agricultural Sciences, North-West University, Mafikeng Campus, Private Bag X2046, Mmabatho 2735, South Africa.

E-mail addresses: 32587139@mynwu.ac.za (O.C. Olatunde), Damian.Onwudiwe@nwu.ac.za (D.C. Onwudiwe).

https://doi.org/10.1016/j.jwpe.2024.105890
Received 15 April 2024; Received in revised form 27 June 2024; Accepted 27 July 2024
Available online 7 August 2024

compounds, suspended solids, and health-threatening coliforms often hinder recycling, necessitating time-consuming and costly treatments [13,16–18]. Traditional wastewater treatment techniques like adsorption and coagulation typically transfer pollutants from one phase to another rather than eliminating them [19]. Other methods, such as chemical treatment, filtration, sedimentation, and membrane technologies, are expensive and can release harmful secondary pollutants into the environment. While chlorination is the most popular and extensively used disinfection method, its byproducts are carcinogenic and mutagenic to human health [20].

These challenges have driven research into advanced oxidation processes (AOPs) as novel water treatment technologies. AOPs generate highly reactive radical species such as H_2O_2, $^{\bullet}OH$, $O_2^{\bullet-}$, O_3, and $SO_4^{\bullet-}$ insitu to degrade inorganic and organic compounds, inactivate water pathogens, and degrade disinfection by-products [21,22]. AOPs include wet oxidation processes, heterogeneous and homogeneous photocatalysis, Fenton and Fenton-like processes, ozonation and electrochemical processes [20]. Heterogeneous photocatalysis, in particular, has proven effective in degrading refractory organics into more minor, biodegradable compounds that can be mineralized into carbon dioxide and water. Furthermore, its potential has been explored in other applications, such as water reduction and H_2O_2 production [23,24] and the synthesis of organic compounds [25].

When light irradiates, a photocatalyst generates numerous holes and electrons that can engage in redox reactions with organic and inorganic pollutants, thereby eliminating contaminants [26,27]. Additionally, the photogenerated holes and electrons can react with O_2 and $H_2O/^{-}$ to generate active oxygen species, such as radicals ($^{\bullet}OH$ and $O_2^{\bullet-}$) and non-radicals ($^1O_2$) [28,29]. Key features of heterogeneous photocatalysis include low operating costs, ambient operating temperature and pressure, and the complete breakdown of target compounds and their intermediates without generating secondary pollutants.

To optimize photocatalytic wastewater treatment, ongoing research aims to identify photocatalysts with enhanced activity. Also, since a significant portion (approximately 43 %) of the solar spectrum comes from the visible light region, visible light-responsive semiconductors are being extensively studied for a wide array of photocatalytic applications [30]. Copper bismuthate ($CuBi_2O_4$) has recently gained attention as a visible-light responsive p-type semiconductor photocatalyst. Discovered by Arai *et al* [31], $CuBi_2O_4$ crystallizes in a tetragonal structure composed of staggered square planar $[CuO_4]^{6-}$ units stacked along the c-axis, with Bi^{3+} ions placed between the stacks and coupled to six O^{2-} ions with three distinct bond distances (Fig. 1a) [32]. This unique structure results in the formation of straight channels around Bi^{3+} ions (Fig. 1b) [33]. The isolated $[CuO_4]^{6-}$ stacks, distinct from the edge-sharing oxygen octahedra or tetrahedra in typical metal oxides, are crucial to $CuBi_2O_4$'s electronic properties [34]. The material is considered an excellent photocatalyst due to its favourable band position, narrow band gap, visible light absorption, low cost, and high flat band potential [35]. However, $CuBi_2O_4$ suffers from a low absorption coefficient, high charge recombination rate, and poor charge transport, stemming from its electronic band structure. For a detailed explanation of $CuBi_2O_4$'s electronic structure, consult the comprehensive review by Gonzaga *et al* [36].

Mitigating the limitations of $CuBi_2O_4$ has received much attention recently to enhance its optoelectronic properties. This is usually achieved through doping [37] or heterostructure formation [38]. The development of semiconductor heterojunctions formed by direct contact between two semiconductors is an effective design to mitigate the limitations faced by single semiconductors [39]. In heterostructure design, extended charge carrier lifetime, increased charge carrier separation, and expanded solar light absorption are facilitated by the coupled semiconductors' appropriate band edge positions. The continual interest in $CuBi_2O_4$ heterostructures, as shown in the publication trend presented in Fig. 1c, attests to the potential of these materials as effective photocatalysts for wastewater treatment. Therefore, this review thoroughly explores copper bismuthate ($CuBi_2O_4$) heterostructures for photocatalytic wastewater treatment, highlighting various synthesis methods and their comparative advantages. The different mechanisms of action of these heterojunctions were explored in detail and the photocatalytic activity of other categories of $CuBi_2O_4$ heterojunctions was discussed. The suggested future research directions also offered valuable insights for developing more efficient and sustainable photocatalysts.

2. Synthesis of $CuBi_2O_4$ heterostructures

Due to its effective light absorption characteristic, copper bismuth oxide ($CuBi_2O_4$) has garnered significant attention in several applications, including photocatalytic degradation of pollutants. However, there have been reports of problems with this Cu-based ternary oxide material, including: (1) fast recombination of photogenerated electron-hole pairs; (2) reduced charge carrier mobility; (3) excessive photostability; and (4) insufficient charge carrier diffusion length. All of this can be addressed effectively by forming a heterojunction interface or other enhancing techniques, such as doping and forming composites [40]. Copper bismuth oxide ($CuBi_2O_4$) and its heterostructures can be fabricated using various methods. These methods include pulsed laser deposition, solid state, solvothermal, electrodeposition, hydrothermal, sol-gel, electrospinning, and spray pyrolysis. Table 1 shows some advantages and disadvantages of the different methods employed in synthesizing $CuBi_2O_4$-based materials. These methods can be employed individually or in combination. Comprehending the chemistry and variables influencing each fabrication method is crucial since they impact the final Cu-based ternary oxide material's structure, morphology, and functionality [41]. Therefore, the application of these techniques to the synthesis of $CuBi_2O_4$ and its heterostructures will be covered in this section.

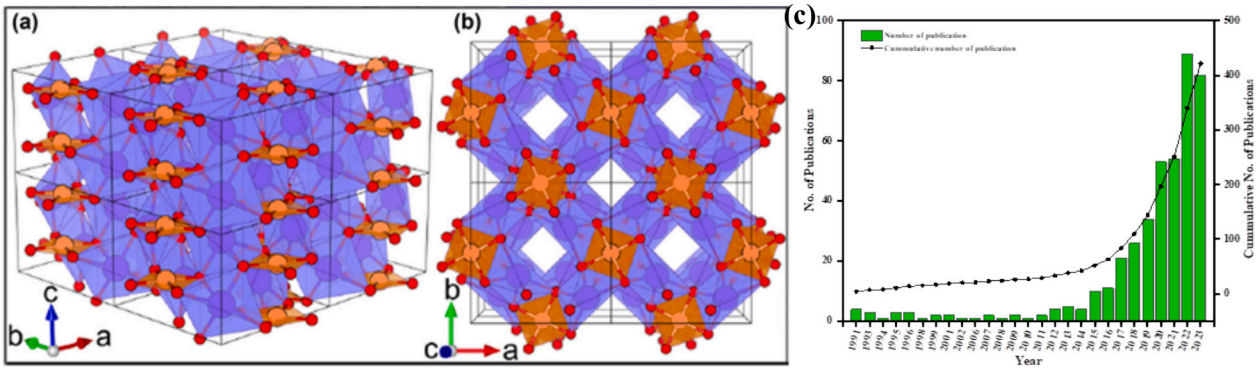

Fig. 1. Isomeric (a) and c-axis projection (b) of $CuBi_2O_4$ crystal structure. Reprinted with permission from ref. [22]. Copyright © 2022 De Gruyter, (c) Publication trend for copper bismuthate from 1991 to 2023.

Table 1
Advantages and disadvantages of $CuBi_2O_4$ synthetic methods.

Fabrication	Advantages	Disadvantages	References
Spray pyrolysis	It can be used for the preparation of pure phases. It's a low-cost preparation method that uses low temperature. Film production cycle is short. Useful for large scale production. Operation of the apparatus is easier and simple.	Affected by extreme temperatures. Chemical stability of the precursor solution is another great issue. Low deposition efficiency. The method uses solvents, molecular precursors, and stabilizers that can be costly and potentially toxic.	[79,80,175,176]
Electrospinning	Simple and effective synthesis route for one-dimensional materials.	The structure morphology has limited control.	[56,71]
Solvothermal method	An easy method with a comparatively low processing temperature. Great degree of repeatability. Advantageous in large-scale manufacturing. Easier to regulate the material's size and shape.	The method requires high volumes of solvents which might be toxic. High-cost equipment such as autoclaves are required. The issue of associated effluent pollution remains a challenging and inevitable issue.	[56,72,177]
Solid state method	Relatively easy usability. it's a solvent-free method. Ability to produce large quantities of synthesized materials.	The required equipment is expensive and the method has a higher percentage of impurities compared to other methods.	[63,69]
Sol gel method	Simple and economical method that uses low sintering temperature.	It takes longer time. Organic solvent used may be toxic.	[43,178]
Hydrothermal method	Simple and cheap method that uses low temperature. No requirement of toxic precursors and solvents. Easier to modify material morphology and size.	Safety issues during fabrication process. The industrial application of this method is restricted by its lengthy preparation time. High cost equipments such as autoclaves are required.	[179,180]
Pulsed laser deposition (PLD)	Quite simple to be carried out and doesn't require post-annealing process. Depositing sharp interfaces between heterojunctions.	The production of high-quality single-crystal thin films presents a significant challenge.	[86,88]
Electrodeposition	Simple and low-cost technique for large area films. The morphology can be significantly manipulated by controlling the synthesis conditions.	Not ideal for large scale applications.	[37,89,90,93,181]

2.1. Hydrothermal method

The hydrothermal approach is the most utilized and versatile technique for fabricating $CuBi_2O_4$ and its heterostructures because of its low temperature, simplicity of use, affordability, uses of low temperature and ability to modify particle size and shape when compared to alternative techniques. It also doesn't require any hazardous or organometallic precursors [42,43]. However, the lengthy preparation period, which might take up to 24 h, restricts the method's industrial applicability. In this synthetic method, the primary precursors utilized in the fabrication of $CuBi_2O_4$ are bismuth (III) nitrate pentahydrate $Bi(NO_3)_3{\cdot}5H_2O$ and Copper(II) nitrate trihydrate $Cu(NO_3)_2{\cdot}3H_2O$. In a study illustrated in Fig. 2a, Zhang *et al* [44] used these precursors for the preparation of $CuBi_2O_4/CdMoO_4$ heterojunctions. A sequence of chemical reactions and reaction eqs. (1–4) resulted in the synthesis of $CuBi_2O_4$ nanoparticles [45]. Rapid hydrothermal synthesis can be facilitated by adding acids like acetic acid and HNO_3 to increase the solubility of $Bi(NO_3)_3{\cdot}5H_2O$. The reaction is often conducted for 0.5–24 h at a temperature between 100 and 200 °C in a stainless steel autoclave lined with Teflon [46,47]. Additionally, alkaline conditions should be used for these reactions to aid in the dissolution-crystallization process, which is the process by which mineralizers attack the amorphous precipitates to form $CuBi_2O_4$ [48].

$$\text{Nucleation } Bi^{3+} + 3OH^- \rightarrow Bi(OH)_3 \quad (1)$$

$$\text{Precipitation } Cu^{2+} + 2OH^- \rightarrow Cu(OH)_2 \quad (2)$$

$$\text{Dehydration } Bi(OH)_3 \rightarrow BiOOH + H_2O \quad (3)$$

$$\text{Crystal growth } 2BiOOH + Cu(OH)_2 \rightarrow CuBi_2O_4 \quad (4)$$

It is often necessary to optimize the Cu/Bi content and reaction time since they affect the final material's morphology, optical absorption properties, and photocatalytic capabilities. Abdulkarem et al. [46] reported the formation of $CuBi_2O_4$ with cubic rod morphology only at specific precursor concentrations and hydrothermal time. In another study, limited hydrothermal duration time resulted in incomplete crystal growth of $CuBi_2O_4$. Extended hydrothermal time eventually displays comparable XRD peaks except for peak intensity. Superior material morphology was achieved through extended hydrothermal duration [49].

Furthermore, the hydrothermal process can be combined with other fabrication techniques. For instance, Xiong *et al* [50] used *in-situ* chemical oxidative polymerization followed by a hydrothermal reaction

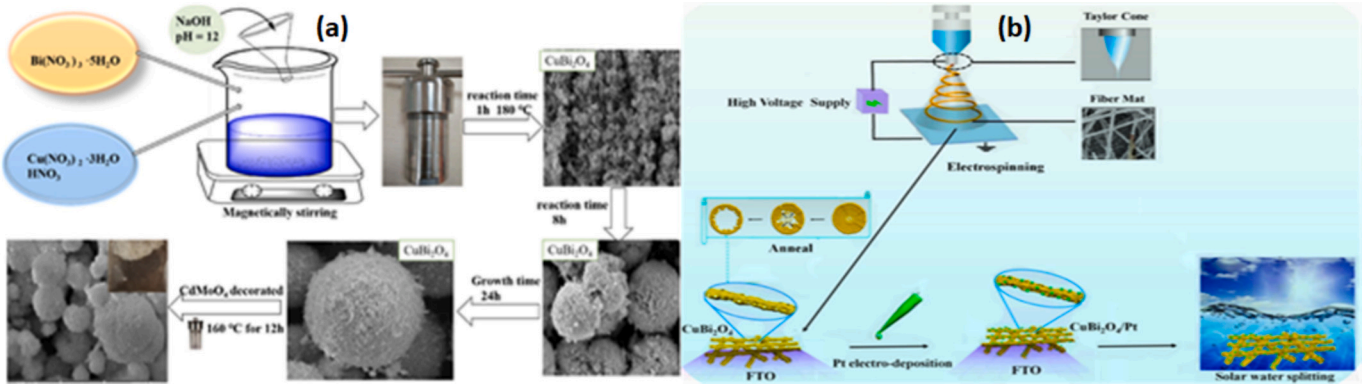

Fig. 2. (a) The preparation of $CuBi_2O_4$/ $CdMoO_4$ heterojunction nanocomposites *via* the hydrothermal treatment. Reproduced from Zhang et al. [44], Copyright © 2021, Elsevier. (b) Synthesis of $CuBi_2O_4$/Pt nanofiber using electrospinning method. Reproduced from Yuan et al. [54], Copyright © 2021 Elsevier.

pathway to fabricate a polyaniline/$CuBi_2O_4$ p-p heterostructure. PANI microsphere was fabricated using *in-situ* chemical oxidative polymerization. Hydrothermal approach was used to fabricate the heterostructure. In another study, Yang *et al* [51] used the hydrothermal method and surface anion exchange method to prepare the *Z*-scheme CuBiOS@ $CuBi_2O_4$ heterojunction.

2.2. Electrospinning

Electrospinning synthesis is an effective and simple synthesis route that is mainly used to fabricate one-dimensional $CuBi_2O_4$ heterostructures through an electrohydrodynamic process [52]. The method forms a jet of polymer solution using an electrified liquid droplet to fabricate the required material [53]. Yuan *et al* [54] reported the fabrication of $CuBi_2O_4$/Pt nanofiber using the electrospinning method. The electrospinning setup contained a high-voltage system and plate collector, as shown in Fig. 2b. Annealing and electro-deposition of Pt completed the fabrication of the heterostructure. Electrospinning rendered the homogenous distribution of the various components on the heterojunction possible [55]. Sometimes, electrospinning can be used in conjunction with other methods to fabricate $CuBi_2O_4$ heterostructures with the precise characteristics that are needed. For example, one-dimensional $CuBi_2O_4$–Bi_2WO_6 was synthesized by electrospinning assisted by solvothermal method [56]. Viscosity and surface tension of the solution are important factors in determining the concentrations needed to achieve continuous post-electrospinning.

2.3. Sol-gel method

The sol-gel method is a versatile technique for fabricating $CuBi_2O_4$ heterostructures. It starts by dissolving precursor molecules in a solvent like alcohol or water. The solution is then heated and stirred, promoting the formation of a gel-like network composed of interconnected nanostructures [57]. This method offers remarkable control over the morphology of $CuBi_2O_4$ heterostructure nanocomposites. By fine-tuning reaction conditions (temperature, stirring) and precursor composition, various morphologies can be achieved, including spheres, irregular shapes, plates, flower-like structures, and even flower-like structures with rod assemblies [58,59]. The sol-gel technique is significantly less complicated than hydrothermal methods. In most cases, the sol-gel method can be combined with other fabrication techniques. For instance, Zhang *et al* [60] used a solution process to fabricate $CuBi_2O_4$. The as-prepared material was turned into $CuBi_2O_4$/TiO_2 p–n heterojunction using the insitu sol-gel coating method. The crystal phase composition, morphology, and interfacial chemical characteristics of the $CuBi_2O_4$/TiO_2 heterojunction synthesized by the sol-gel technique have been reported to be influenced by changes in the precursors' molar ratio of Cu/Bi and the calcination temperature. The sol-gel method can be modified to the Pechini method through complexing cations in an aqueous-organic medium [61]. Due to its homogenous ion distribution and utilization of inexpensive materials, the Pechini sol-gel technique has been investigated recently for the synthesis of $CuBi_2O_4$ heterojunctions. This technique also involves the addition of additives like gelling agents. In one instance, copper nitrate, bismuth nitrate, polybasic acids, and gelling agents were used to fabricate $CuBi_2O_4$/Bi_3ClO_4 nanocomposites using an improved Pechini sol-gel process [58].

2.4. Solid state method

The solid-state route preparation for $CuBi_2O_4$ heterostructures takes place *via* mechanical milling and mechanochemical synthesis from solid reagents [62]. Each of these methods has its advantages and shortcomings. Mechanical milling is the most widely utilized of these due to its ease of use, affordability, solvent-free environment, and capacity to generate substantial amounts of synthesized materials [63,64]. However, the method requires high monitoring and control against contaminations during mechanical milling. Merely using water as a dispersion and carrying out multiple annealing processes with different intermediate milling stages can enhance precursor mixture homogeneity and decrease powder particle size through mechanical milling [65]. Multiple annealing cycles can establish strong bonds between solid precursors, facilitating charge transfer across surfaces [66]. Chen *et al* [67] reported the fabrication of $CuBi_2O_4$/MWCNT composites by mixing solid precursors, followed by a ball-milling reaction. The synthesis of $CuBi_2O_4$ heterostructures through a solid-state response involving mechanical milling of different ratios of $CuBi_2O_4$ and CeO_2 was also reported by Elaziouti *et al* [68]. This method is affected by the surface area, reactivity, and free energy change of the reactants.

2.5. Solvothermal method

The solvothermal method is a widely adopted traditional and robust route for fabricating $CuBi_2O_4$ and its heterostructures. The solvothermal method is a straightforward and efficient technique for fabricating nanostructured materials. Its benefits include large-scale production, low cost, high reproducibility, relatively low processing temperature, and the capability to control the material's size and morphology with the help of appropriate additives [69,70]. The method also uses both water and organic solvents. $CuBi_2O_4$ heterostructures have been prepared using ultrapure water, glycerol, ethylene glycol, and ethanol. These have been used to modify the coordination of solvated species, induce specific structures, and increase the mobility of the dissolved ions [71–73]. The Solvothermal method is carried out in a closed reaction vessel that is heated above the boiling point of the solvents being used, such as a sealed autoclave lined with Teflon. $CuBi_2O_4$ heterojunction materials can be synthesized in one or two steps using solvothermal methods. The

most common methods are the one-step ones [74]. Muthukrishnaraj *et al* [75] successfully fabricated a reduced graphene oxide/$CuBi_2O_4$ heterostructure using a single-step solvothermal process. A mixture of graphene oxide and $CuBi_2O_4$ precursor solutions was placed in a Teflon-lined autoclave and heated for 24 h at 180 °C during synthesis. Reactant chemical reactivity and the solvothermal reaction kinetics in the solvothermal method can be improved by combining it with other technologies like microwaves, electrospinning, mechanical mixing, sonochemistry, and others [76]. For instance, using a solvothermal-assisted electrospinning method, Teng, Li [56] fabricated a one-dimensional Bi_2WO_6/$CuBi_2O_4$ heterojunction. The solvothermal method was used to fabricate Bi_2WO_6, while $CuBi_2O_4$ heterojunction material was fabricated by the electrospinning method under a high voltage**.** Chemical parameters like the composition, characteristics, and pH of the solvent and precursor, as well as thermal parameters like pressure and temperature, can impact solvothermal reactions [77,78].

2.6. Spray pyrolysis

Fabrication of $CuBi_2O_4$ heterostructures by spray pyrolysis involves spraying precursor solution on a heated substrate. The sprayed droplets undergo thermal degradation due to the heat from the heated surface. The desired heterostructures are formed by sintered and crystallized constituent elements that have recombined because of heat breakdown. Spray pyrolysis has been used to deposit $CuBi_2O_4$ heterostructures on a variety of substrates, including metals, glass (Fluorine Tin oxide-coated glass substrate), and ceramics [79]. Water scavengers (such as trimethyl orthoacetate and triethyl orthoformate) and additives like polyethylene glycol can be added to the precursor solution to enhance sprayed droplet dispersal characteristics and avoid the quick hydrolysis and polycondensation of bismuth ions [80]. The structural and optical characteristics of the synthesized heterostructures are influenced by the spray drying temperature, the pace at which the droplets evaporate, the concentration of the solution, and the preparative conditions. Shi *et al* [81] examined the impact of temperature during spray-drying on the growth of Bi_2O_3 nanoparticles on $CuBi_2O_4$. Results showed increased spray-drying temperature increased the peak intensity of 020 facets in the composites. As the temperature of the spray-drying process rose, the precursor's crystallization also progressively improved. High temperatures can efficiently shorten the time needed for the segregation gradient to form, resulting in pure-phase films. However, high temperatures can cause the supporting substrate to melt and the deposited film to adhere to the substrate poorly [82]. As with other fabrication methods, spray pyrolysis can be combined with other methods. For example, Wang *et al* [83] used the diffusion-assisted spray pyrolysis procedure to manufacture self-doped $CuBi_2O_4$.

2.7. Pulsed laser deposition

Pulsed laser deposition (PLD) is another method that has been used to fabricate $CuBi_2O_4$ heterostructures. The method's fundamental component is the high-intensity pulsed laser beam that is used to deposit a layer on the target material. As opposed to previously discussed methods, this method is carried out at a very high vacuum with the presence of a background gas [84]. Woo *et al* [85] reported the synthesis of $CuBi_2O_4$ thin-film photocathodes by pulsed laser deposition using pure Bi_2O_3 and CuO. Different oxygen partial pressures were used to manipulate stoichiometry. Combining PLD and other techniques, such as rapid thermal processing, can also be used to control the Bi: Cu stoichiometry [86]. In another study, Lee *et al* [87] used the pulsed laser deposition method to fabricate $CuBi_2O_4$/NiO thin film photocathodes. The synthesized material was reported to have a dense, homogeneous, flat surface that removes pores and voids in heterostructures. However, $CuBi_2O_4$ heterostructure thin film formed by the PLD method was in a polycrystalline rather than a single crystalline state. Therefore, to fabricate single-crystal thin films of $CuBi_2O_4$, it is important to optimize the lattice misfit strain between the target material and the substrate [88].

2.8. Electrodeposition

The electrodeposition method has also been used to prepare $CuBi_2O_4$ and its heterostructures with excellent photoelectrochemical properties [89–91]. In a study reported by Nakabayashi *et al* [92], CuO and Bi_2O_3 precursors were co-deposited by anodic electrolysis on a conductive fluorine tin oxide-coated glass substrate (FTO). After that, the formed $CuBi_2O_4$ films were heated for 4 h at 500 °C. Before electrodeposition, the conductive substrate's surface was cleansed using air plasma. During the electrodeposition procedure, the clean FTO serves as the anode. The electrolyte solution's composition, bath concentration, electrodeposition time, and PLD deposition potential pulse count should all be optimized for the fabrication of pure material [93,94] and regulation of the thickness of the obtained material [45]. Electrodeposition can be combined with other techniques in the preparation of $CuBi_2O_4$ and its heterostructures. For instance, Liu *et al* [95] fabricated $CuBi_2O_4$/$BiVO_4$ p-n heterojunction using a combination of pulsed laser and electrodeposition.

3. $CuBi_2O_4$ heterostructures and mechanism of action

The main idea behind creating a semiconductor-based photocatalytic heterostructure is to maximize overall photocatalytic performance by a logical arrangement of component materials to fully utilize the benefits of each component. The photocatalytic process comprises three basic complementary and indispensable steps [96]: (1) generation of electron-hole pairs by light irradiation when the energy of the incident photons is larger than the bandgap energy ($h\upsilon > E_g$), electron promotion to the conduction band occurs [97]. (2) separation of photogenerated charge carriers; under the coulombic forces of attraction; the timescale for photogenerated electron-hole pair recombination is $<10^{-9}$ femtoseconds [98] and the efficiency of the photocatalytic process is hampered by this reverse recombination of charge carriers; (3) charge transfer onto catalytic sites for redox reaction; the buildup of charge carriers on the photocatalytic surface may result in unintended semiconductor instability due to the presence of highly oxidative holes and reductive electrons. The valence band maximum and conduction band minimum positions determine the oxidation and reduction potential of photogenerated electrons and holes, respectively. A shallow valence band and high conduction band position are the preference for photocatalytic degradation processes.

Based on the aforementioned fundamental steps of photocatalysis, broad light absorption and strong redox ability are two important properties of the photocatalytic activity of a semiconductor. However, both properties are mutually exclusive since narrowing of E_g is essential for broad light absorption, while band gap widening (highly positive valence and negative conduction bands) results in strong redox ability [99]. Therefore, to mitigate this obstacle, the development of heterojunction has proven effective. In heterojunction formation, appropriate band edge positions are advantageous for longer charge carrier lifetime, broader light absorption, and improved charge carrier separation [100].

3.1. Charge transfer mechanism in $CuBi_2O_4$ heterostructures

Based on the material composited with $CuBi_2O_4$, enhanced charge carrier lifetime and properties are achieved through charge transfer mechanisms such as type II, *Z*-scheme, S-scheme, plasmonic effect, Schottky junction or carbon-based electron sinks. While type II, Z-scheme, and S-scheme charge transfer mechanisms are associated with $CuBi_2O_4$/semiconductor heterostructures, plasmonic effect and Schottky junction are observed in $CuBi_2O_4$/metal composites.

In $CuBi_2O_4$/semiconductor heterostructures, the disparity in band energy potential results in three different types of band alignment: (1)

straddling gap, (2) broken gap, and (3) staggered gap, as shown in Fig. 3a. However, in practice, only staggered heterojunctions can enhance charge transport [101]. A staggered gap heterojunction can be formed by combining semiconductors of the same or different types. Many studies reveal that the heterojunction formed by combining p-type and n-type semiconductors with staggered energy gaps is more efficient in improving photocatalytic activity [102–104]. This improvement is primarily attributed to the existence of a built-in electric field. Creating a built-in electric field arising from the majority carrier diffusion effect at the interface which interferes with the photogenerated charge carrier transport in p-n heterojunctions [105]. This has been explored in limiting charge carrier recombination and enhancing photocatalytic activity [106,107]. According to Che et al. [101], p-n heterojunction can be of two types. In the first type of p-n heterojunction, the fermi level of the reduction p-type semiconductor is relatively large, while the n-type semiconductor has relatively small Fermi energy. Local band bending occurs after the compounding of the semiconductors, leading to the flow of electrons from the oxidation n-type semiconductor to the p-type semiconductor until the equilibration of the Fermi levels. This establishes an internal electric field (IEF) directed from the n-type semiconductor to the p-type. The transfer mode of photogenerated charge carriers could follow the type II, *Z*-scheme, or S-scheme pathway based on the influence of IEC and band structure.

The other type of p-n heterostructure is formed from n-type semiconductors with small conduction bands (CB) and p-type semiconductors with large valence bands (VB). In this structure, IEF is developed similarly to what was described earlier. The charge transfer mechanism in this heterostructure is either by type II or *Z*-scheme mechanism. However, the Z-scheme is the most prevalent in this type of p-n heterojunction. The electrostatic force generated by the IEF due to p-n heterojunction can improve the transfer of photogenerated charge carriers. For $CuBi_2O_4$ heterostructures, this type of p-n heterojunction is prevalent in dual Z-scheme materials.

3.1.1. *Type II $CuBi_2O_4$/semiconductor heterostructures*

In a typical type II heterojunction, photogenerated electrons migrate from the CB of the semiconductor with the higher potential to the CB of the semiconductor with a lower CB. In contrast, the flow of photogenerated holes follows the opposite direction [108]. The occurrence of this charge transfer remains debatable due to the role played by the IEF and the work function-induced interfacial band bending [109]. The major difference between the type II charge transfer mechanism and the other mechanisms is the direction of the generated IEF, as shown in Fig. 3b. While the direction of the IEF is from the reduction photocatalyst to the oxidation photocatalyst in S-Scheme and *Z*-scheme charge transfer, the IEF flows in the opposite direction in type II heterojunctions. Despite the ability of the type II charge transfer mechanism to suppress charge carrier recombination, this is usually at the expense of the redox ability of the photocatalyst, which weakens the photocatalytic reaction's driving force.

In the study by Li *et al* [110], *in-situ* mechanochemical fabrication of p-n $Bi_2MoO_6/CuBi_2O_4$ heterojunction with type-II charge transfer mechanism was reported. The $CuBi_2O_4$ CB experienced an upward shift, while the Bi_2MoO_6 VB underwent a downward shift, leading to Fermi level equilibration during the mechanochemical process. These shifts were accompanied by the creation of an IEF that formed in the direction of Bi_2MoO_6 to $CuBi_2O_4$. Under visible light irradiation, the photogenerated electrons on the CB of $CuBi_2O_4$ were inclined to transfer to the CB of Bi_2MoO_6 due to the influence of the IEF. Similarly, the photogenerated holes on the VB of Bi_2MoO_6 transferred to the VB of $CuBi_2O_4$. The effective movement of electron-hole pairs ultimately led to the exceptional photocatalytic ability of the $Bi_2MoO_6/CuBi_2O_4$ heterojunction. The Mott-Schottky plot confirmed the p-type in $CuBi_2O_4$ and p-n-type heterojunction in $Bi_2MoO_6/CuBi_2O_4$, while the photoluminescence spectra of the heterojunction showed increased charge carrier lifetime, compared to $CuBi_2O_4$ and Bi_2MoO_6.

Other $CuBi_2O_4$/semiconductor type II heterojunctions that have been proposed include $CuBi_2O_4/ZnFe_2O_4$ [111], $CuBi_2O_4$/CuO [112], and AgI/$CuBi_2O_4$ [113]. Recently, type II heterojunctions have also been proposed for $CuBi_2O_4$/metal heterostructures such as n-Si/$CuBi_2O_4$ [114].

3.1.2. *S-scheme $CuBi_2O_4$/semiconductor heterostructures*

Similar to the type II mechanism, the S-scheme mechanism also relies on establishing direct electrical contact between two semiconductors. When two semiconductors with dissimilar band structures are interfaced, Fermi level (E_f) equilibration occurs due to charge redistribution. Band bending must, therefore, occur in the space charge zone. This produces an internal electric field, which makes it easier for electrons and holes to separate in the region [116]. The holes flow to the more negative site, while electrons flow to the more positive region. The valence band and conduction band of both semiconductors determine the direction of band bending [117]. The upward band bending increases the oxidation ability by attracting holes, while the downward band bending promotes reduction reactions by concentrating electrons onto the surface. The S-scheme mechanism thus leads to effective charge separation, while preserving the semiconductors' redox ability [118]. The mechanistic scheme for S-scheme charge transfer is shown in Fig. 4 (a).

The S-scheme charge transfer mechanism was proposed for $CuBi_2O_4/CoV_2O_6$ with $CuBi_2O_4$ acting as the reduction photocatalyst while CoV_2O_6 was the oxidation photocatalyst [119]. The flow of electrons after contact between the two materials was from $CuBi_2O_4$, which has the higher Fermi level, to CoV_2O_6, with the lower Fermi level, until Fermi level equilibration is achieved. This led to the upward bending of the $CuBi_2O_4$ band edge due to electron loss and producing electron

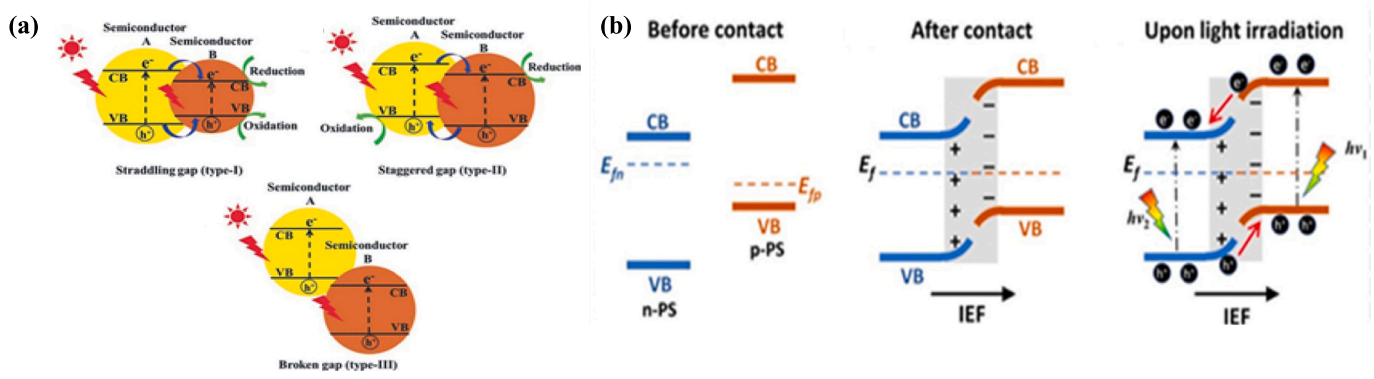

Fig. 3. (a) Band alignment in semiconductor-semiconductor heterojunctions. Reproduced from Che et al. [101]. Copyright ©, 2023 Elsevier. (b) Mechanistic scheme for type II charge transfer heterojunction. Reprinted with permission from Schumacher *et al* [115].

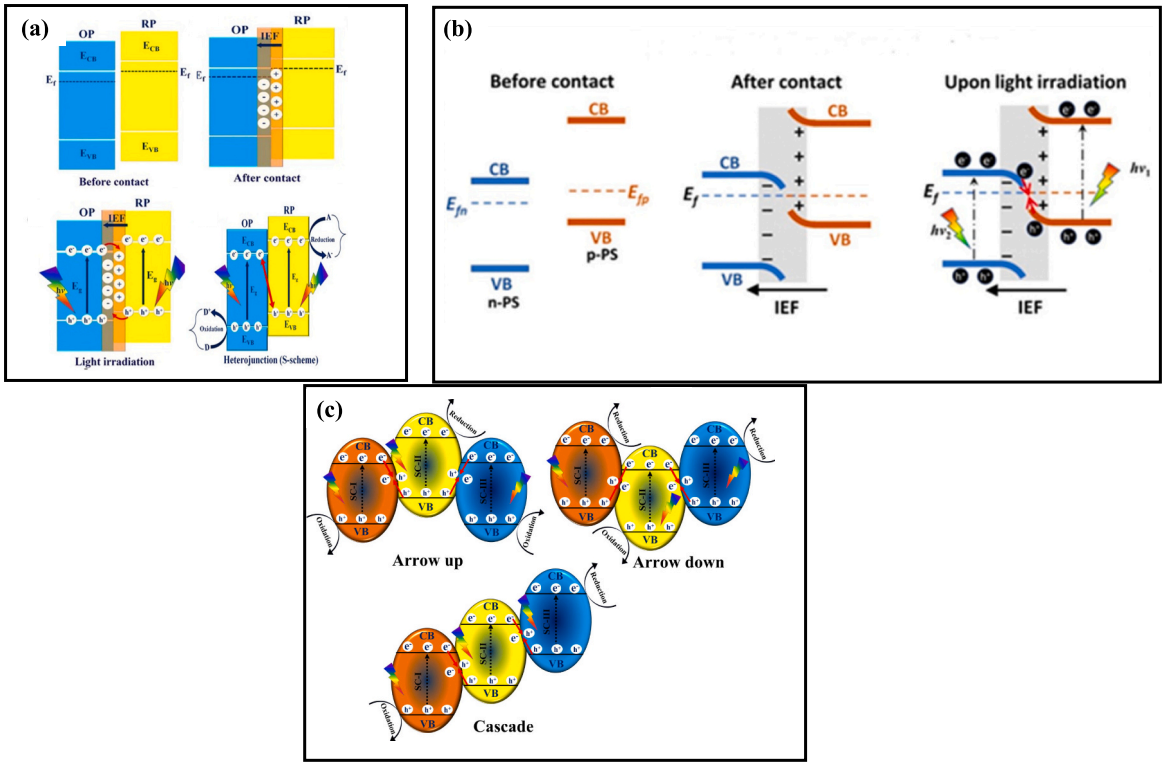

Fig. 4. (a) S-scheme charge transfer mechanism. Adapted from Hasija et al. [117], Copyright © 2021 Springer (b) Mechanistic scheme for *Z*-scheme charge transfer heterojunction. Reprinted with permission from Schumacher et al. [115], Copyright © 2022 Springer (c) Dual Z-scheme charge transfer configurations, adapted from Kumar et al. [132], Copyright © 2022, Elsevier.

depletion region. In contrast, the reception of electrons by CoV_2O_6 led to the downward bending of the band edge with the corresponding establishment of IEF from $CuBi_2O_4$ to CoV_2O_6. Under light irradiation, photogenerated electrons in the CB of CoV_2O_6 combine with holes in the valence band of $CuBi_2O_4$ resulting in the preservation of the electrons in the CB of $CuBi_2O_4$ and holes in the VB of CoV_2O_6.

The S-scheme mechanism has recently gained much attention in understanding the improved photocatalytic activity of $CuBi_2O_4$ heterostructures. Other S-scheme $CuBi_2O_4$ heterojunctions that have been reported include $CuBi_2O_4$/BiOBr [120], Bi_2WO_6/$CuBi_2O_4$ [121], and α-Fe_2O_3/$CuBi_2O_4$ [122].

3.1.3. *Z-scheme $CuBi_2O_4$/semiconductor heterostructures*

The Z-scheme mechanism mimics the natural photosynthesis process. The traditional Z-scheme mechanism involves the transfer of electrons between the semiconductors through a shuttle redox mediator (electron acceptor/donor pair such as Fe^{3+}/Fe^{2+} or IO_3/I^-)) [123–125]. In 2006, the all-solid-state Z-scheme was introduced in which noble metals, or conductive materials such as graphene and carbon nanotubes, acted as the electron mediator. The *Z*-scheme mechanism relies on forming low-contact resistant ohmic contact at the semiconductor interface arising from a conductor or large surface defects [126]. The photogenerated holes in the semiconductor with a higher valence band edge combine with photogenerated electrons in the semiconductor with a lower conduction band edge through the ohmic contact. Furthermore, the electrons located at the higher CB edge and the holes at the lower VB edge will be conserved for the reduction and oxidation reactions, respectively as shown in Fig. 4(b).

In their study on $CoFe_2O_4$/$CuBi_2O_4$ p-n heterostructure as nanophotocatalyst for C(OH)-H bond activation, Ghobadifard *et al* [127], reported a *Z*-scheme charge transfer mechanism. A shift in the VB and CB of $CuBi_2O_4$ to more negative values was observed compared to those of $CoFe_2O_4$. The study confirmed the electron migration from the CB of $CoFe_2O_4$ to combine with holes in the VB of $CuBi_2O_4$, thus preserving photogenerated charge carriers with high redox potential for enhanced catalytic activity. The radical scavenging experiment significantly supported the proposed *Z*-scheme mechanism.

In real Z-scheme heterojunctions, the electron and hole transfer pathway may sometimes differ from the proposed mechanism, reducing its efficiency. This is, however, circumvented by developing multicomponent Z-scheme systems for improved photocatalytic performance, such as the dual Z-scheme systems. Charge carrier separation efficiency is further enhanced because of the multiple charge transfer routes in dual Z-scheme heterojunctions compared to traditional Z-scheme systems [128]. Three different charge transfer configurations have been identified for the dual Z-scheme heterojunctions: arrow up configuration, arrow down configuration, and cascade configuration (Fig. 4(c)). The difference among the configurations lies in the band alignment and the resulting enhancement in the redox ability of the heterojunction. In the arrow up configuration, the band edges of the semiconductor in the middle are higher than those of the other two.

In contrast, in the arrow-down configuration, the band edges of the middle semiconductor are lower than the other semiconductors [129,130]. In the cascading configuration, the band edges of the middle semiconductor lie between those of the other two semiconductors [131]. Furthermore, the arrow-up configuration leads to enhanced oxidative ability, while the arrow-up configuration results in more reductive ability. For the cascade configuration, the photocatalyst's oxidative and reductive ability are enhanced [132].

Mafa *et al* [133] designed a novel Co_3O_4/$CuBi_2O_4$/$SmVO_4$ dual Z-scheme heterostructure photocatalyst with enhanced charge transfer efficiency for improved degradation of carbamazepine under visible light irradiation. The improved catalytic activity of the heterojunction compared to the pristine materials was due to the enhanced charge separation in the heterojunction, which is significant for improving catalytic activity. The Z-scheme mechanism results in photogenerated

electrons in $CuBi_2O_4$ and $SmVO_4$ recombined with holes in Co_3O_4, leading to the preservation of holes in the VB of $CuBi_2O_4$ and $SmVO_4$ and electrons in the CB of Co_3O_4.

3.1.4. Schottky junction and plasmonic resonance $CuBi_2O_4$ heterostructures

Integrating semiconductors with noble metals is a widely employed strategy to exploit their charge kinetics. The metal may serve several roles in enhancing photocatalytic performance; however, in terms of charge transfer, two main mechanisms are involved in this heterostructure type: the plasmonic effect and the Schottky junction. While the plasmonic effect does not require direct contact between the metal and the semiconductor, direct contact is significant for the Schottky junction [134]. These two mechanisms depend on the photocatalytic system, such as the types of metal and semiconductor, as well as the wavelengths of incident light, and may operate either in conjunction or independently [116].

Schottky junctions are developed when a metal and a semiconductor make an interface and the metal's work function is higher than that of the semiconductor. In that case, electrons flow from the semiconductor to the metal, accompanied by a simultaneous formation of space-charge region. This leads to the semiconductor band's upward bending, and the space charge region facilitates charge separation and enhances electron and hole transport (Fig. 5a-c)). Metal loading is an important factor to be considered in developing a Schottky junction, as more metal does not correlate to more Schottky barriers. High metal loading may lead to a larger number of electron trapping sites and may also reduce the semiconductor's exposure to light [135].

When plasmonic metals such as gold (Au), silver (Ag), and copper (Cu) are doped onto semiconductors, their surface plasmonic resonance (SPR) effect can be explored in photocatalysis since these surface plasmons resonate within UV–visible light [136,137]. Surface plasmon refers to the coordinated movement of conduction electrons at the boundary between a conductor and an insulator. It involves three primary mechanisms (Fig. 5(d)): 1) resonant photon scattering by metal, 2) creation of plasmon resonance energy transfer (PRET), which is an intense oscillating electric field around the metal, and 3) generation of hot electron-holes in the metal [138].

In the report by Shi *et al* [140], the visible-light-driven photocatalytic activity of $Au/CuBi_2O_4$ heterostructure showed the involvement of both the plasmonic effect and Schottky junction in the enhancement of the photocatalytic activity of the composite. The plasmonic effect of Au was evident in the enhanced absorption of the composite in the UV and visible regions. Simultaneously, the hot electrons generated by Au through surface plasmon resonance (SPR) can be transferred to the conduction band of $CuBi_2O_4$, resulting in increased charge carrier generation. While there are a few metal-$CuBi_2O_4$ heterostructures such as $Pt/CuBi_2O_4$ [141], $Pd@CuBi_2O_4$ [142], $Ag\text{-}CuBi_2O_4$ [143], not much attention has been paid to the charge transfer mechanisms in these heterostructures. It is, therefore, imperative to understand these processes in metal-$CuBi_2O_4$ heterostructures for highly effective heterostructures of this class to be discovered.

4. $CuBi_2O_4$-based heterojunctions in wastewater treatment

4.1. $CuBi_2O_4$/transition metal oxide heterostructures

$CuBi_2O_4$/transition metal oxide heterostructures are one of the most explored heterojunctions for photocatalytic degradation of pollutants. Recently, Zhang *et al* [144] reported the synthesis of a 0D/1D $CuBi_2O_4@WO_3$ heterojunction fabricated through the electrospinning method. The method achieved a uniform distribution of $CuBi_2O_4$ nanoparticles on WO_3 nanofibers while ensuring intimate contact between the nanoparticles and the nanofibers, which was significant for charge transfer and separation enhancement. Energy level difference calculation showed that while $CuBi_2O_4$ was the reduction photocatalyst, WO_3 was the oxidation photocatalyst, implying electron migration from $CuBi_2O_4$ to WO_3 to achieve Fermi level equilibration. This establishes a built-in electric field at the composite interface, which is consistent with the S-scheme charge transfer mechanism. The successful establishment of the charge transfer scheme resulted in efficient charge transfer across the heterostructure interface, reducing the recombination of photogenerated charge carriers while also enhancing the light-absorbing ability of the composite. The enhanced charge carrier property of the heterostructure was evidenced in the improved photocatalytic activity, achieving 70 % degradation efficiency for tetracycline, compared to 31 % and 16 % achieved by $CuBi_2O_4$ and WO_3, respectively.

Zinc oxide (ZnO) is another well explored metal oxide photocatalyst because of its non-toxicity, high chemical and thermal stability, strong oxidation ability and low-cost [145]. Its applicability is, however, limited by its wide band gap energy, fast charge carrier recombination and low visible light utilization [146]. Sabri *et al* [147], however, showed in their study that the formation of $ZnO/CuBi_2O_4$ heterostructure could benefit from improved visible light absorption, large surface area and p-n heterojunction formation at the interface of the semiconductors to achieve improved photocatalytic activity for different dyes. The charge transfer mechanism reportedly followed the type II mechanism, which significantly enhanced charge transfer and separation as supported by the photoluminescence spectra, electrochemical impedance spectroscopy, and transient photocurrent response of the material. In the presence of persulfate anion, the photocatalytic activity of the $ZnO/CuBi_2O_4$ catalyst was significantly enhanced due to the reaction of photogenerated electrons with $S_2O_4^{2-}$ to produce $SO_4^{\bullet-}$ radical. Therefore, in addition to the generation of a highly powerful radical species, the separation of the photogenerated charge carrier was simultaneously enhanced.

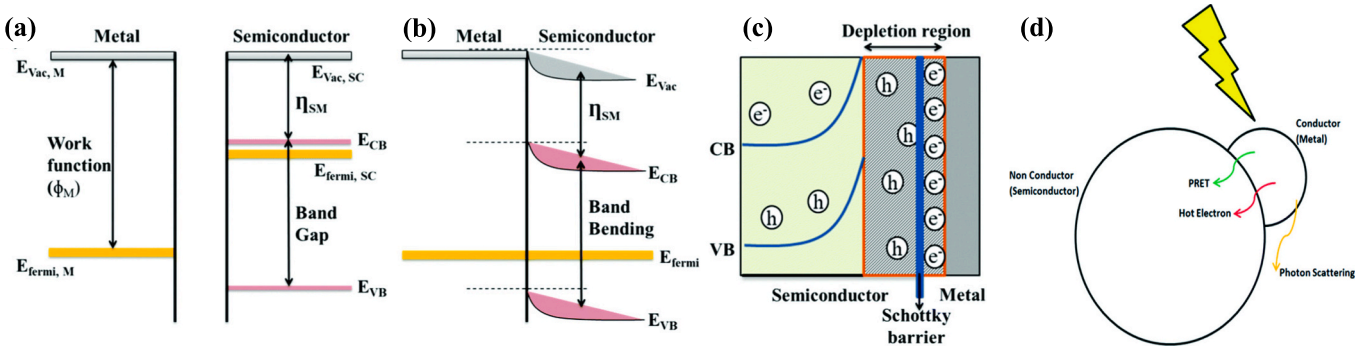

Fig. 5. Mechanistic scheme for Schottky heterostructures (a) metal and semiconductor band structure before contact, (b) band structure of metal and semiconductor after contact (c) charge carrier flow and depletion region formation at the metal-semiconductor interface and (d) Surface plasmon resonance mechanism. Reprinted with permission from [139]. Copyright Royal Society of Chemistry.

Other reported $CuBi_2O_4$/metal oxide heterostructures with improved photocatalytic activity for wastewater treatment include $CuBi_2O_4/TiO_2$ [71,148], $Co_3O_4/CuBi_2O_4$ [149], $CuBi_2O_4$/SrO [150] and α-Fe_2O_3/$CuBi_2O_4$ [151]. Table 2 presents a summary of the photocatalytic activity of some $CuBi_2O_4$ heterostructures. These heterostructures generally leverage the enhancement of charge carrier separation and increased surface area to achieve increased efficiency in the photocatalytic degradation of wastewater.

4.2. $CuBi_2O_4$/ oxyhalide heterostructure

Bismuth-based ternary oxyhalides such as BiOBr, BiOI and BiOCl have recently been considered potential photocatalysts for wastewater purification [152]. Due to their layered structure and indirect band gap, BiOX allows for the generation of the intrinsic internal electric field, which aids charge carrier separation [153]. The formation of $CuBi_2O_4$/BiOX heterostructure has a high prospect of exhibiting improved photocatalytic activity as shown in literature such as $CuBi_2O_4$/BiOBr/Biochar [154], $CuBi_2O_4$/Bi/BiOBr [155] and N-BiOBr/$CuBi_2O_4$ [72]. The amplification of reactive oxygen species generation by 5%Bi_3O_4Br/$CuBi_2O_4$ was demonstrated by Tian *et al* [156], while exploring the heterojunction in a PS/Vis light system for tetracycline degradation. Electron paramagnetic resonance (EPR) analysis confirmed the generation of a high level of $^{\bullet}OH$ and $^1O_2$ species, which accounted for the high activity of the catalysts. The type II charge transfer mechanism was observed to be responsible for increasing photogenerated charge carrier separation and transient photocurrent with the subsequent generation of radical species.

The improved photocatalytic activity of $CuBi_2O_4$/BiOCl was reported by Qiu *et al* [157] for the photocatalytic degradation of tetracycline hydrochloride. The 20 % $CuBi_2O_4$ weight composition was reported to show enhanced activity, which is 58.2 and 4.1 times those of $CuBi_2O_4$ and BiOCl, respectively. The enhanced visible light absorption and the improved separation of photogenerated charge carriers due to the built-in electric field accounted for the improved activity. The type II charge transfer mechanism was observed to be prevalent in the p-n heterojunction (Fig. 6(a)), with a charge transfer from the n-type BiOCl to the p-type $CuBi_2O_4$ confirmed from the X-ray photoelectron spectroscopy analysis (Fig. 6(b)). The improved charge carrier property of the heterostructure was also confirmed by the smaller radius of the EIS spectra and the reduced intensity of the PL compared to the individual compounds (Fig. 6(c&d)).

4.3. $CuBi_2O_4$/ternary metal oxide heterostructure

Ternary metal oxides with multiple oxidation states have demonstrated superior photocatalytic activity compared to binary metal oxides. This is due to their ability to undergo multiple redox reactions during electrochemical processes [158]. Typically, the valence band of ternary metal oxide semiconductors combines the O 2p orbital with a d0 or d10 orbital of a metal cation [159]. The additional metal cation in the ternary metal oxide contributes an orbital that plays a part in forming its conduction band. The hybridization of the O 2p orbital with the metal orbital results in the elevation of the valence bands of ternary metal oxides, leading to a slight reduction in their band gaps compared to binary metal oxides. This reduction in band gap energy makes ternary metal oxides suitable materials for heterojunction formation. Some reported $CuBi_2O_4$/ternary metal oxide include $CuBi_2O_4/ZnFe_2O_4$ [111], $Bi_2WO_6/CuBi_2O_4$ [160], $BiFeO_3$@$CuBi_2O_4$ [161] and $CoTiO_3/CuBi_2O_4$ [162].

Ternary metal oxides with piezoelectric effect, such as $AgNbO_3$, could play an essential role in achieving charge carrier separation due to the depolarization electric field arising from the spontaneous polarization of ferroelectrics and the piezoelectric potential generated under stress. This phenomenon was demonstrated by Huang *et al* [163] in their study on the piezo-photocatalytic performance of $CuBi_2O_4/AgNbO_3$ heterojunction for degrading rhodamine B dye. The study affirmed that the piezo-phototronic coupling effect in the polarized catalyst greatly improved the separation of charge carriers, leading to enhanced activity for organic dye degradation.

A novel $Bi_2SiO_5/CuBi_2O_4$ heterojunction with high oxygen vacancies was explored for the photocatalytic inactivation of *E. coli* and the

Table 2
Summary of the photocatalytic activity of some $CuBi_2O_4$ heterojunction photocatalysts.

Heterojunction	Pollutant	Process Parameters	Charge transfer mechanism	Efficiency %	Kinetic rate (min^{-1})	Ref
$CuBi_2O_4$/CuO	Methylene blue Metronidazole	Visible light, 50 mg, 30 mg/L, 25 mL	Type II	100 36	11×10^{-4} 36×10^{-4}	[182]
Ag@$Bi_2O_3/CuBi_2O_4$	17α-ethinylestradiol Cr(VI)	Visible light (250 W, Xe lamp), 40 mg, 10 mg/L, 100 mL	S-Scheme	94.6 96.9	1.8×10^{-2} 1.1×10^{-2}	[183]
$CuBi_2O_4/In_2O_3$	Methylene blue	Visible light (300 W, Xe lamp), 50 mg, 10 mg/L, 50 mL	Z-Scheme	97	3.2×10^{-2}	[184]
$Sb_2O_3/CuBi_2O_4$	Methylene blue Acid Blue	Visible light (400 W, metal halide lamp), 10 mg, 10 mg/L, 20 mL	Z-Scheme	90 83	–	[185]
$CuBi_2O_4/TiO_2$	Cr(VI)	Visible light, 100 mg, 30 mg/L, 100 mL	–	98	1.4×10^{-2}	[186]
$CuBi_2O_4/WO_3$	Tetracycline	Visible light (500 W, Xenon lamp), 50 mg, 20 mg/L, 50 mL	Z-Scheme	90	1.7×10^{-2}	[187]
$CuBi_2O_4/MoS_2$	Tetracycline	Visible light (300 W, Xenon lamp), 50 mg, 10 mg/L, 100 mL	Type II	76	9.5×10^{-3}	[188]
$BiFeO_3/CuBi_2O_4$/$BaTiO_3$	Norfloxacin	Visible light (500 W, Xenon lamp), 20 mg, 10 mg/L, 20 mL	Z-scheme	93	1.1×10^{-1}	[189]
$CuBi_2O_4/Bi_2Sn_2O_7$/Sn_3O_4	Tetracycline	Visible light (300 W, Xenon lamp), 100 mg, 20 mg/L, 100 mL	Z-Scheme	85	3.9×10^{-1}	[190]
$CuBi_2O_4$/Bi/BiOBr	Methylene blue (MB)	Visible light (500 W, Xenon lamp), 50 mg, 5 mg/L, 100 mL	Z-scheme	73	5.2×10^{-3}	[155]
$NaNbO_3/CuBi_2O_4$	Rhodamine B	Visible light (250 W, Xe lamp), 40 mg, 10 mg/L, 100 mL	Polarized electron transfer	75	1.1×10^{-2}	[191]
$Bi_2MoO_6/CuBi_2O_4$	Ciprofloxacin	Visible light (500 W, Xe lamp), 200 mg, 10 mg/L, 200 mL	Type II	90.2	1.2×10^{-2}	[110]
$CuBi_2O_4$ /Bi_2WO_6	Tetracycline	Visible light (300 W, Xenon lamp), 50 mg, 20 mg/L, 50 mL	Z-Scheme	93	2.8×10^{-2}	[179]
$CuBi_2O_4/ZnFe_2O_4$	Tetracycline	Visible light (300 W, Xe lamp), 100 mg, 20 mg/L, 100 mL	Type II	80.1	1.2×10^{-2}	[192]
$Bi_2WO_6/CuBi_2O_4$	Tetracycline	Visible light (300 W, Xe lamp), 50 mg, 15 mg/L, 100 mL	Z-Scheme	91	2.7×10^{-2}	[77]

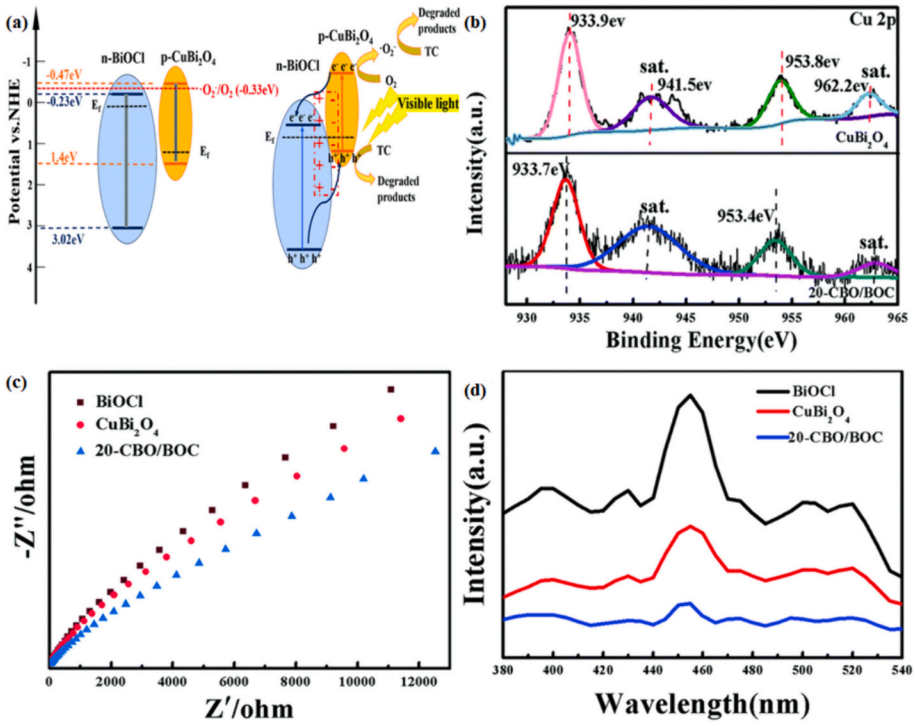

Fig. 6. (a) Proposed charge transfer mechanism for $CuBi_2O_4$/BiOCl (b) XPS spectra of the Cu 2p orbital of $CuBi_2O_4$ and $CuBi_2O_4$/BiOCl-the shift in the binding level of the energy confirms the charge transfer from BiOCl to $CuBi_2O_4$ (c) EIS spectra of BiOCl, $CuBi_2O_4$ and $CuBi_2O_4$/BiOCl and (d) Photoluminescence spectra of BiOCl, $CuBi_2O_4$ and $CuBi_2O_4$/BiOCl. Adapted from ref. [140]. Copyright © 2022 RSC.

photocatalytic degradation of tetracycline by Yu *et al* [164]. Bi_2SiO_5 is considered a suitable material for heterostructure due to its strong stability and non-toxicity. Its layered structure facilitates photogenerated charge carrier migration and oxidation reactions [165,166]. Improved light absorption properties and charge carrier separation efficiency were observed in the heterostructure due to the formation of oxygen vacancies and the *Z*-scheme charge transfer mechanism. The heterojunction attained 83.3 % degradation of tetracycline after 2 h while completely inactivating the *E. coli* in 2.5 h. Fig. 6 shows the characterization of the photogenerated charge carriers of the $Bi_2SiO_5/CuBi_2O_4$. The heterojunction showed a higher photocurrent response (Fig. 7(a)) compared to $CuBi_2O_4$ and Bi_2SiO_5, signifying improved charge carrier separation and migration. Fig. 7(b) shows the EIS measurement of the catalysts, showing the heterojunction had a smaller charge transfer resistance and high separation efficiency. Furthermore, the improved charge carrier separation was confirmed by the significant reduction in the intensity of the PL spectra of the heterojunction (Fig. 7(c)), while

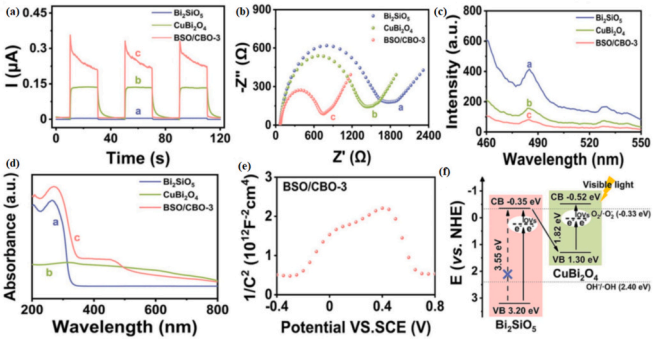

Fig. 7. (a) photocurrent response (b) Nyquist plot, (c) PL spectra (d) UV–vis Drs of Bi_2SiO_5, $CuBi_2O_4$ and BSO/CBO, (e) Mott-Schottky and (f) charge transfer mechanism of BSO/CBO heterostructure. Adapted from Yu et al. [164]. Copyright © 2023 Elsevier.

Fig. 7(d) shows the higher absorption capacity of the heterojunction and the extension of the band edge into the visible region. From Fig. 7(e), the inverted V-shape of the Mott-Schottky plot showed the formation of a p-n heterojunction, with the Z-scheme charge transfer mechanism shown in Fig. 7(f).

Table 2 summarises the photocatalytic activity of some $CuBi_2O_4$/ternary oxides heterostructures. These materials' photocatalytic activity benefited from the redox activity of the ternary metal oxides, resulting in enhanced pollutant degradation.

4.4. $CuBi_2O_4$/carbon nanostructure heterostructure

Carbon-based materials such as graphene, graphene oxide, reduced graphene oxide, and carbon nanotubes possess good electrical conductivity and can thus act as an electron sink for semiconductor materials [167–170]. Also, the high surface area of these materials enhances the adsorption properties of the composites, which is a crucial factor in applications such as photocatalysis. In explaining the improved photocatalytic activity of MWCNT/$CuBi_2O_4$, Chen et al. [67] proposed the transfer of photogenerated electrons from $CuBi_2O_4$ into MWCNT, which resulted in enhanced charge separation and a subsequent improvement in photocatalytic activity. A simultaneous improvement in visible light absorption was also observed in the MWCNT/$CuBi_2O_4$ heterostructure. A similar charge transfer mechanism was reported for $CuBi_2O_4$/rGO by Annamalai *et al* [171]. Carbon-based materials could also act as electron transfer bridges between two semiconductors as reported by Dutta et al. [143] and Zhou et al. [154]. According to the report by Dutta *et al* [172], CNTs could act as an electron transfer bridge between $AgBiO_3$ and $CuBi_2O_4$ in a *Z*-scheme CNTs@$CuBi_2O_4$/$AgBiO_3$ leading to improved light absorption and improved charge separation and transport.

The purpose of forming a $CuBi_2O_4$/carbon heterostructure photocatalyst is to enhance electron-hole pair separation and use photocatalysis's redox potential. It has been observed that this $CuBi_2O_4$ heterostructure exhibits superior efficiency in pollutant degradation [173]. Muthukrishnaraj et al. [75] fabricated reduced graphene oxide/

$CuBi_2O_4$ heterojunction through a solvothermal technique. The incorporation of graphene oxide resulted in strong absorption in the visible region. This resulted in outstanding degradation for methylene blue and methyl orange, with 87 % and 95 % degradation efficiencies, respectively. The elevated catalytic effectiveness of the heterostructure may be ascribed to effective separation of photo-induced hole-electron pairs, enhanced surface area, enhanced adsorption capability, and π–π interaction with graphene, hence promoting rapid degradation. In another study, and Shi [174] reported the fabrication of $CuBi_2O_4$/g-C_3N_4 p–n heterojunction, which was thereafter used to remove tetracycline from wastewater. In comparison with pristine $CuBi_2O_4$ and g-C_3N_4, the $CuBi_2O_4$/g-C_3N_4 heterojunctions demonstrated enhanced photocatalytic activity in the degradation of TC. The increased photocatalytic activity was also attributed to three factors: (1) stronger visible light absorption, (2) larger hierarchical surface area; and (3) promoted charge carrier separation and transfer.

4.5. $CuBi_2O_4$/inorganic polymer hybrid heterostructure

The hybrid heterostructure of $CuBi_2O_4$ and inorganic polymer is one of the least explored $CuBi_2O_4$ heterostructures in the photocatalytic degradation of pollutants. Xiong et al. [50] reported the fabrication of polyaniline/$CuBi_2O_4$ composite for photocatalytic reduction of Cr(VI). The enhanced photo-reduction performance of the synthesized photocatalyst on Cr(VI) was ascribed to increased specific surface area for pollutants adsorption and desorption, the reduced recombination of charges, and the effective transfer of charges across the interface. Similarly, Ahmad *et al* [174] reported the degradation of ammonia by $CuBi_2O_4$/polyaniline composite fabricated *via in situ* polymerization of aniline with pre-synthesized $CuBi_2O_4$ composites. The study showed that 96 %, 78 % and 70 % of ammonia was degraded in 180 mins under visible light by $CuBi_2O_4$/polyaniline composite PANI and $CuBi_2O_4$, respectively. The strong absorption intensity in the visible range and the effective charge transfer of photogenerated electrons and holes are responsible for the heterostructure composite material's increased ammonia degradation. In comparison to pure materials, the composite material also demonstrated remarkable stability.

4.6. $CuBi_2O_4$ ternary heterojunctions

Several $CuBi_2O_4$ ternary heterojunctions have been studied as potential photocatalysts for the degradation of different pollutants. In contrast to pure $CuBi_2O_4$, $CuBi_2O_4$ ternary heterojunctions effectively separate photogenerated electrons and holes and broaden the light absorption range [44,58]. A dual *Z*-scheme heterojunction photocatalyst, Co_3O_4/$CuBi_2O_4$/$SmVO_4$, with effective activity for tetracycline degradation was reported by Mafa et al. [133]. The ternary material showed higher activity than the binary compositions of the explored materials. This showed a high synergy within the ternary material, which accounted for the improved charge carrier transport and separation. In another study, Hou et al. [78] studied the degradation of rhodamine B and methylene blue using a ternary Bi_2O_3–CuO–$CuBi_2O_4$ photocatalyst. The photoluminescence (PL) experiment was used to establish the ideal material composition for the composite material. It revealed a decreased

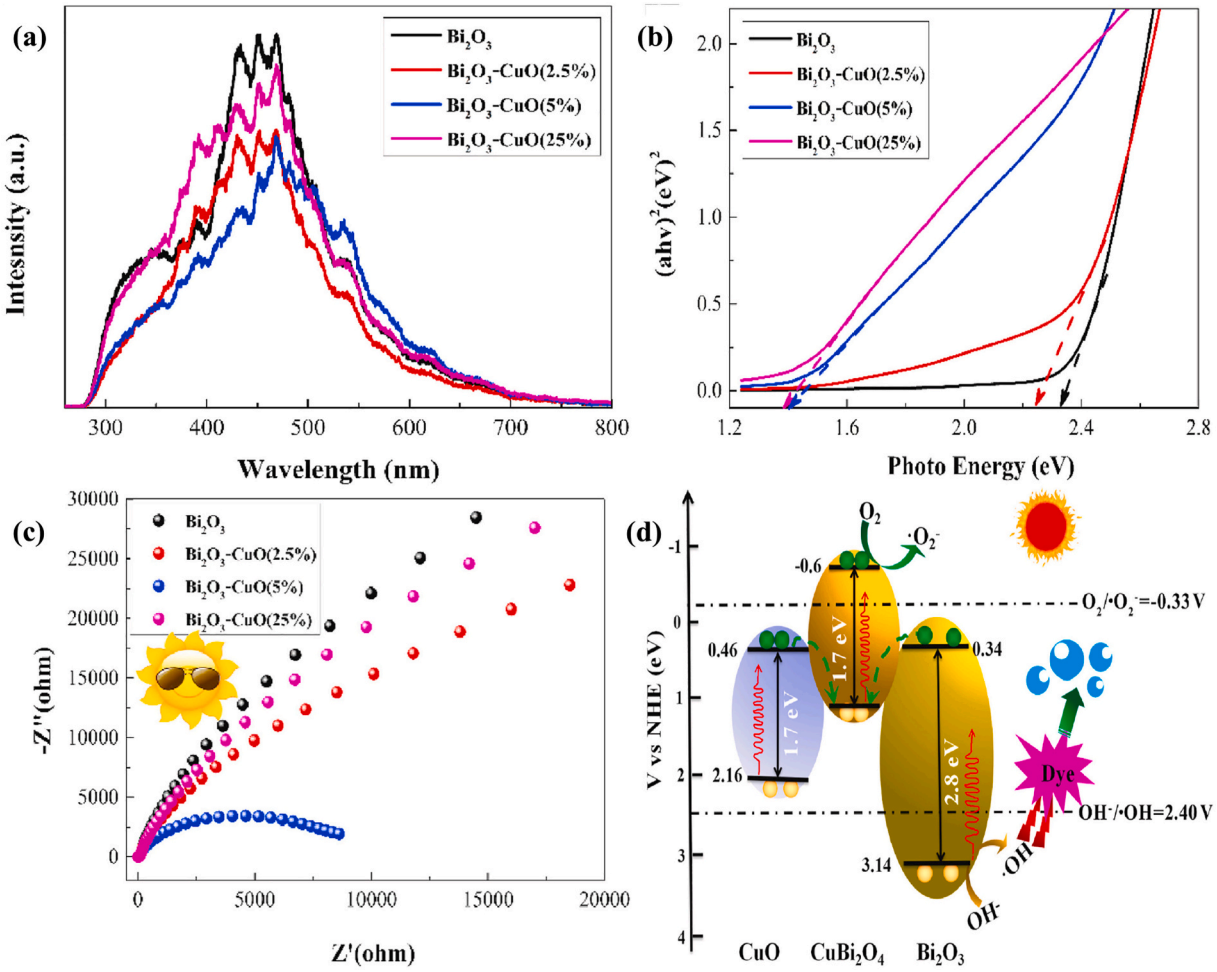

Fig. 8. a) PL spectra of photocatalytic materials (b) Kubelka-Munk plots, (c) EIS and (d) Charge transfer scheme for Bi_2O_3–CuO–$CuBi_2O_4$. Adapted from ref. [78]. Copyright © 2022, Elsevier.

PL peak intensity (Fig. 8(a)) in the composite with Bi_2O_3–CuO (5 %) with the 5 % Cu/Bi concentration ratio, indicating reduced electron-hole recombination. Furthermore, as demonstrated by the band gap energies in Fig. 8(b), it was found that a small amount of CuO added to the heterostructure might increase the absorption intensity throughout the visible spectrum. The EIS measurement of the photocatalysts in Fig. 8(c) demonstrates that Bi_2O_3–CuO (5 %) heterojunction had the greatest separation efficiency and lowest charge transfer resistance. The photocatalytic study demonstrated that the ternary catalyst was able to achieve 100 % solar-driven photocatalytic degradation efficiency in 140 min for RhB and 60 min for MB, respectively, through the utilization of hydroxyl radicals (·OH) and superoxide anions ($O_2^{\bullet-}$) as illustrated in Fig. 8d. The photocatalytic performance of pristine materials was much lower than that of ternary catalysts.

5. Future challenges and prospects

Photocatalytic degradation of pollutants is one of the most potent options for improving the quality and availability of potable water for human consumption. Therefore, developing semiconductor materials with suitable optical properties has become a significant endeavour. Recently, $CuBi_2O_4$ has gained much attention because of its environmental friendliness and unique optical properties. However, like most semiconductors, it also suffers from inadequate light absorption and high charge carrier recombination, which has led to the exploration of its heterojunctions.

The applicability of $CuBi_2O_4$-heterojunction in wastewater treatment is constrained by several key issues that need to be investigated further. Firstly, a proper understanding of the interfacial properties of the heterojunction and how it influences the photocatalytic properties. To optimize the potential of these heterojunctions fully, a clear understanding of interfacial interaction and charge transfer at this interface needs to be clearly understood. This enables the understanding of the intrinsic mechanism of the enhanced photocatalytic activity of these heterojunctions. As demonstrated in the review, understanding the mechanisms behind the longer charge carrier lifespan and greater charge carrier separation in $CuBi_2O_4$ heterostructures is vital for their practical application.

Secondly, there is a need to investigate the built-in electric field generated in $CuBi_2O_4$-based heterojunctions. Due to the lack of appropriate characterization techniques, providing evidence for this phenomenon is difficult. Attempts at using *in-situ* XPS and advanced microscopic techniques may offer an indirect route to studying this effect.

Finally, there is a need to explore data-driven investigations of $CuBi_2O_4$-based heterojunctions, as this may provide a shorter route to identifying highly effective $CuBi_2O_4$-heterojunctions. Integrating machine learning and high-throughput screening in materials science could accelerate the discovery of optimal heterojunction configurations and processing conditions.

As environmental protection continues to gain more attention, identifying semiconductor photocatalysts with enhanced activity will become necessary. The potential of $CuBi_2O_4$-based heterojunctions makes them promising for further exploration in obtaining highly effective photocatalytic materials. Continuous research and development, mainly focusing on these heterojunctions' synthesis methods and interfacial properties, will be critical in overcoming the current challenges and realizing their full potential in environmental remediation applications.

6. Conclusion

The review highlights the significant potential of $CuBi_2O_4$ heterostructures in the photocatalytic degradation of water pollutants. $CuBi_2O_4$ heterostructures exhibit remarkable photocatalytic properties due to their enhanced solar light absorption, extended charge carrier lifespan, and efficient charge carrier separation. Various synthesis methods provide a versatile toolkit for optimizing performance. The advancements in this field hold great promise for developing sustainable and effective solutions for water purification, contributing to public health and environmental protection. Future research should address challenges such as stability, scalability, exploring novel synthesis techniques, and conducting real-world application trials. The promising results and future advancements in $CuBi_2O_4$ heterostructures are crucial for achieving efficient water purification.

CRediT authorship contribution statement

Olalekan C. Olatunde: Writing – original draft, Conceptualization. **Lawrence Sawunyama:** Writing – original draft, Conceptualization. **Tunde L. Yusuf:** Conceptualization, Writing – review & editing. **Damian C. Onwudiwe:** Writing – review & editing, Supervision, Funding acquisition.

Declaration of competing interest

The authors declare that they have no known competing financial interests or personal relationships that could have appeared to influence the work reported in this paper.

Data availability

No data was used for the research described in the article.

References

[1] M.N. Chong, B. Jin, C.W.K. Chow, C. Saint, Recent developments in photocatalytic water treatment technology: a review, Water Res. 44 (10) (2010) 2997–3027.
[2] M.H. Ahmadi Azqhandi, M. Foroughi, Z. Gholami, Efficient removal of levofloxacin by a magnetic NiFe-LDH/N-MWCNTs nanocomposite: characterization, response surface methodology, and mechanism, Environ. Res. 215 (2022) 113967.
[3] S.F. Noorani Khomeyrani, B. Ghalami-Choobar, M.H. Ahmadi Azqhandi, M. Foroughi, An enhanced removal of para-nitrophenol (PNP) from water media using CaAl-layered double hydroxide-loaded magnetic g-CN nanocomposite, J. Water Process Eng. 46 (2022) 102516.
[4] S. Malato, P. Fernández-Ibáñez, M.I. Maldonado, J. Blanco, W. Gernjak, Decontamination and disinfection of water by solar photocatalysis: recent overview and trends, Catal. Today 147 (1) (2009) 1–59.
[5] T. Wintgens, F. Salehi, R. Hochstrat, T. Melin, Emerging contaminants and treatment options in water recycling for indirect potable use, Water Sci. Technol. 57 (1) (2008) 99–107.
[6] S. Suárez, M. Carballa, F. Omil, J.M. Lema, How are pharmaceutical and personal care products (PPCPs) removed from urban wastewaters? Rev. Environ. Sci. Biotechnol. 7 (2008) 125–138.
[7] C. Byrne, G. Subramanian, S.C. Pillai, Recent advances in photocatalysis for environmental applications, J. Environ. Chem. Eng. 6 (3) (2018) 3531–3555.
[8] R. Fagan, D.E. McCormack, D.D. Dionysiou, S.C. Pillai, A review of solar and visible light active TiO_2 photocatalysis for treating bacteria, cyanotoxins and contaminants of emerging concern, Mater. Sci. Semicond. Process. 42 (2016) 2–14.
[9] S. Deylami, M.H. Sabzevari, M. Ghaedi, M.H.A. Azqhandi, F. Marahel, Efficient photodegradation of disulfine blue dye and tetracycline over robust and green g-CN/Ag3VO4/PAN nanofibers: experimental design, RSM, RBF-NN and ANFIS modeling, Process Saf. Environ. Prot. 169 (2023) 71–81.
[10] S. Mishra, R. Acharya, K., Parida spinel-ferrite-decorated graphene-based nanocomposites for enhanced photocatalytic detoxification of organic dyes in aqueous medium: a review, Water 15 (2023), https://doi.org/10.3390/w15010081.
[11] A. Rafiq, M. Ikram, S. Ali, F. Niaz, M. Khan, Q. Khan, M. Maqbool, Photocatalytic degradation of dyes using semiconductor photocatalysts to clean industrial water pollution, J. Ind. Eng. Chem. 97 (2021) 111–128.
[12] M.S. Fakhri B, N. Ghassemi Barghi, M. Moradnia Mehdikhanmahaleh, S.M.M. Raeis Zadeh, T. Mousavi, R. Rezaee, M. Daghighi, M. Abdollahi, Pharmaceutical wastewater toxicity: an ignored threat to the public health, Sustain. Environ. 10 (1) (2024) 2322821.
[13] S.A.A.A.N. Almuktar, S.N. Abed, M. Scholz, Wetlands for wastewater treatment and subsequent recycling of treated effluent: a review, Environ. Sci. Pollut. Res. 25 (24) (2018) 23595–23623.
[14] T. Asano, F. Burton, T. Tsuchihashi, G., Water Reuse–Issues, Technologies and Applications, Metcalf & Eddie Inc, 2007.

[15] J.D. Contreras, R. Meza, C. Siebe, S. Rodríguez-Dozal, Y.A. López-Vidal, G. Castillo-Rojas, R.I. Amieva, S.G. Solano-Gálvez, M. Mazari-Hiriart, M.A. Silva-Magaña, Health risks from exposure to untreated wastewater used for irrigation in the Mezquital Valley, Mexico: a 25-year update, Water Res. 123 (2017) 834–850.

[16] M. Foroughi, M.H.A. Azqhandi, A biological-based adsorbent for a non-biodegradable pollutant: modeling and optimization of Pb (II) remediation using GO-CS-Fe_3O_4-EDTA nanocomposite, J. Mol. Liq. 318 (2020) 114077.

[17] E. Yazdankish, M. Foroughi, M.H.A. Azqhandi, Capture of I131 from medical-based wastewater using the highly effective and recyclable adsorbent of g-C_3N_4 assembled with Mg-Co-Al-layered double hydroxide, J. Hazard. Mater. 389 (2020) 122151.

[18] M. Foroughi, M.H. Ahmadi Azqhandi, S. Kakhki, Bio-inspired, high, and fast adsorption of tetracycline from aqueous media using Fe_3O_4-g-CN@PEI-β-CD nanocomposite: modeling by response surface methodology (RSM), boosted regression tree (BRT), and general regression neural network (GRNN), J. Hazard. Mater. 388 (2020) 121769.

[19] S. Radmehr, M. Hosseini Sabzevari, M. Ghaedi, M.H. Ahmadi Azqhandi, F. Marahel, Adsorption of nalidixic acid antibiotic using a renewable adsorbent based on graphene oxide from simulated wastewater, J. Environ. Chem. Eng. 9 (5) (2021) 105975.

[20] R. Dewil, D. Mantzavinos, I. Poulios, M.A. Rodrigo, New perspectives for advanced oxidation processes, J. Environ. Manage. 195 (2017) 93–99.

[21] G. Liu, J. Ji, H. Huang, R. Xie, Q. Feng, Y. Shu, Y. Zhan, R. Fang, M. He, S. Liu, X. Ye, D.Y.C. Leung, UV/H_2O_2: An efficient aqueous advanced oxidation process for VOCs removal, Chem. Eng. J. 324 (2017) 44–50.

[22] Y.-d. Chen, X. Duan, X. Zhou, R. Wang, S. Wang, N.-q. Ren, S.-H. Ho, Advanced oxidation processes for water disinfection: features, mechanisms and prospects, Chem. Eng. J. 409 (2021) 128207.

[23] L. Acharya, G. Swain, B.P. Mishra, R. Acharya, K. Parida, Development of $MgIn_2S_4$ microflower-embedded exfoliated B-doped g-C_3N_4 nanosheets: p–n heterojunction Photocatalysts toward photocatalytic water reduction and H2O2 production under visible-light irradiation, ACS Appl. Energy Mater. 5 (3) (2022) 2838–2852.

[24] R. Acharya, P. Pani, Visible light susceptible doped TiO_2 photocatalytic systems: an overview, Mater. Today Proc. 67 (2022) 1276–1282.

[25] M. Curti, D.W. Bahnemann, C.B. Mendive, Mechanisms in heterogeneous photocatalysis: titania under UV and visible light illumination, in: Reference Module in Materials Science and Materials Engineering, Elsevier, 2016.

[26] S.-W. Lv, X. Wang, X. Wei, Y. Zhang, Y. Cong, L. Che, Introduction of cluster-to-metal charge transfer in UiO-66-NH_2 for enhancing photocatalytic degradation of bisphenol a in the existence of peroxymonosulfate, Sep. Purif. Technol. 292 (2022) 121018.

[27] H. Li, H. Zhu, Y. Shi, H. Shang, L. Zhang, J. Wang, Vacancy-rich and porous NiFe-layered double hydroxide ultrathin nanosheets for efficient photocatalytic NO oxidation and storage, Environ. Sci. Technol. 56 (3) (2022) 1771–1779.

[28] Y. Cong, X. Chen, L. Ye, X. Li, S.-W. Lv, A newly-designed free-standing $NiCo_2O_4$ nanosheet array as effective mediator to activate peroxymonosulfate for rapid degradation of emerging organic pollutant with high concentration, Chemosphere 307 (2022) 136073.

[29] Z.H. Jabbar, B.H. Graimed, Recent developments in industrial organic degradation via semiconductor heterojunctions and the parameters affecting the photocatalytic process: a review study, J. Water Process Eng. 47 (2022) 102671.

[30] S. Mishra, L. Acharya, B. Marandi, K. Sanjay, R. Acharya, Boosted photocatalytic accomplishment of 3D/2D hierarchical structured $Bi_4O_5I_2$/g-C_3N_4 p-n type direct Z-scheme heterojunction towards synchronous elimination of Cr(VI) and tetracycline, Diamond Relat. Mater. 142 (2024) 110834.

[31] T. Arai, Y. Konishi, Y. Iwasaki, H. Sugihara, K. Sayama, High-throughput screening using porous photoelectrode for the development of visible-light-responsive semiconductors, J. Comb. Chem. 9 (4) (2007) 574–581.

[32] S.P. Berglund, F.F. Abdi, P. Bogdanoff, A. Chemseddine, D. Friedrich, R. van de Krol, Comprehensive evaluation of $CuBi_2O_4$ as a photocathode material for photoelectrochemical water splitting, Chem. Mater. 28 (12) (2016) 4231–4242.

[33] J.K. Cooper, Z. Zhang, S. Roychoudhury, C.-M. Jiang, S. Gul, Y.-S. Liu, R. Dhall, A. Ceballos, J. Yano, D. Prendergast, $CuBi_2O_4$: electronic structure, optical properties, and photoelectrochemical performance limitations of the photocathode, Chem. Mater. 33 (3) (2021) 934–945.

[34] H.J. Jung, Y. Lim, B.-U. Choi, H.B. Bae, W. Jung, S. Ryu, J. Oh, S.-Y. Chung, Direct identification of antisite cation intermixing and correlation with electronic conduction in $CuBi_2O_4$ for photocathodes, ACS Appl. Mater. Interfaces 12 (39) (2020) 43720–43727.

[35] M. Kumar, B. Meena, P. Subramanyam, D. Suryakala, C., Subrahmanyam emerging copper-based semiconducting materials for photocathodic applications in solar driven water splitting, Catalysts 12 (2022), https://doi.org/10.3390/catal12101198.

[36] I.L.E. Gonzaga, C.C. Mercado, Copper ternary oxides as photocathodes for solar-driven CO_2 reduction 61 (1) (2022) 430–457.

[37] D. Kang, J.C. Hill, Y. Park, K.-S. Choi, Photoelectrochemical properties and photostabilities of high surface area $CuBi_2O_4$ and Ag-doped $CuBi_2O_4$ photocathodes, Chem. Mater. 28 (12) (2016) 4331–4340.

[38] Y.-H. Lai, K.-C. Lin, C.-Y. Yen, B.-J. Jiang, A tandem photoelectrochemical water splitting cell consisting of $CuBi_2O_4$ and $BiVO_4$ synthesized from a single Bi_4O_5 I_2 nanosheet template, Faraday Discuss. 215 (2019) 297–312.

[39] S. Zhong, Y. Xi, Q. Chen, J. Chen, S. Bai, Bridge engineering in photocatalysis and photoelectrocatalysis, Nanoscale 12 (10) (2020) 5764–5791.

[40] H. Zhang, J. Xue, J. Han, Y. Ling, Photo-assisted Fenton reactions and growth evolution of crack-urchined $CuBi_2O_4$ microspheres assembled by nanorods, Ceram. Int. 46 (15) (2020) 23742–23748.

[41] T.O. Ajiboye, A.A. Mafolasire, S. Lawrence, N. Tyhali, S.D. Mhlanga, Composite and pristine silver bismuth sulphide: synthesis and up-to-date applications, J. Inorg. Organomet. Polym. Mater. (2023) 1–25.

[42] Y. Zhang, H. Yang, W. Wang, H. Zhang, R. Li, X. Wang, R. Yu, A promising supercapacitor electrode material of $CuBi_2O_4$ hierarchical microspheres synthesized via a coprecipitation route, J. Alloys Compd. 684 (2016) 707–713.

[43] J. Zhang, Y. Jiang, Preparation, characterization and visible photocatalytic activity of $CuBi_2O_4$ photocatalyst by a novel sol–gel method, J. Mater. Sci. Mater. Electron. 26 (2015) 4308–4312.

[44] X. Zhang, S. Wang, L. Lin, X. Tan, Y. Zeng, Design of a novel $CuBi_2O_4$/$CdMoO_4$ heterojunctions with nano-microsphere structure: synthesis and photocatalytic degradation mechanism, Colloids Surf. A Physicochem. Eng. Asp. 614 (2021) 126008.

[45] Y. Wang, H. Wang, A.R. Woldu, X. Zhang, T. He, Optimization of charge behavior in nanoporous $CuBi_2O_4$ photocathode for photoelectrochemical reduction of CO_2, Catal. Today 335 (2019) 388–394.

[46] A. Abdulkarem, J. Li, A. Aref, L. Ren, E. Elssfah, H. Wang, Y. Ge, Y. Yu, $CuBi_2O_4$ single crystal nanorods prepared by hydrothermal method: growth mechanism and optical properties, Mater. Res. Bull. 46 (9) (2011) 1443–1450.

[47] G. Sharma, Z. Zhao, P. Sarker, B.A. Nail, J. Wang, M.N. Huda, F.E. Osterloh, Electronic structure, photovoltage, and photocatalytic hydrogen evolution with p-$CuBi_2O_4$ nanocrystals, J. Mater. Chem. A 4 (8) (2016) 2936–2942.

[48] A.S. Mary, C. Murugan, A. Pandikumar, Uplifting the charge carrier separation and migration in Co-doped $CuBi_2O_4$/TiO_2 pn heterojunction photocathode for enhanced photoelectrocatalytic water splitting, J. Colloid Interface Sci. 608 (2022) 2482–2492.

[49] X. Zhang, S. Wang, C. Pan, Y. Zeng, Construction of Ag/$CuBi_2O_4$/Ag_2MoO_4 composites for enhanced degradation of methylene blue and the proposed possible photocatalytic mechanism, Mater. Lett. 288 (2021) 129388.

[50] J. Xiong, H.-Y. Zeng, C.-R. Chen, D.-Y. Peng, S. Xu, D.-S. An, Conjugated hollow polyaniline/$CuBi_2O_4$ composite with enhanced photocatalytic activity under visible-light, Surf. Interfaces 29 (2022) 101804.

[51] L. Yang, J. Wang, T. Ma, L. Zhang, Nanointerface engineering Z-scheme CuBiOS@$CuBi_2O_4$ heterojunction with OS interpenetration for enhancing photocatalytic hydrogen peroxide generation and accelerating chromium (VI) reduction, J. Colloid Interface Sci. 611 (2022) 760–770.

[52] F. Yang, X. Yu, Z. Liu, J. Niu, T. Zhang, J. Nie, N. Zhao, J. Li, B. Yao, Preparation of Z-scheme $CuBi_2O_4$/Bi_2O_3 nanocomposites using electrospinning and their enhanced photocatalytic performance, Mater. Today Commun. 26 (2021) 101735.

[53] J. Xue, T. Wu, Y. Dai, Y. Xia, Electrospinning and electrospun nanofibers: methods, materials, and applications, Chem. Rev. 119 (8) (2019) 5298–5415.

[54] X. Yuan, Y. Liu, H. Yuan, B. Liu, T. Guo, H. Zhou, X. Li, An electrospun porous $CuBi_2O_4$ nanofiber photocathode for efficient solar water splitting, Polymers 13 (19) (2021) 3341.

[55] L. Zhang, Q. Shen, F. Huang, L. Jiang, J. Liu, J. Sheng, Y. Li, H. Yang, Electrospinning directly synthesis of 0D/1D $CuBi_2O_4$@ WO_3 nanofiber photocatalyst with S-scheme heterojunction, Appl. Surf. Sci. 608 (2023) 155064.

[56] P. Teng, Z. Li, S. Gao, K. Li, M. Bowkett, N. Copner, Z. Liu, X. Yang, Fabrication of one-dimensional Bi_2WO_6/$CuBi_2O_4$ heterojunction nanofiber and its photocatalytic degradation property, Opt. Mater. 121 (2021) 111508.

[57] D. Bokov, A. Turki Jalil, S. Chupradit, W. Suksatan, M. Javed Ansari, I. H. Shewael, G.H. Valiev, E. Kianfar, Nanomaterial by sol-gel method: synthesis and application, Adv. Mater. Sci. Eng. 2021 (2021) 1–21.

[58] H. Najafian, F. Manteghi, F. Beshkar, M. Salavati-Niasari, Fabrication of nanocomposite photocatalyst $CuBi_2O_4$/Bi_3ClO_4 for removal of acid brown 14 as water pollutant under visible light irradiation, J. Hazard. Mater. 361 (2019) 210–220.

[59] A. Sokhansanj, M. Haghighi, M. Shabani, Macroporous flowerlike $Bi_2O_2CO_3$-$CuBi_2O_4$ nanoheterojunction photocatalyst for high concentrated malachite green degradation: influence of nanocomposite composition and sonication approach, J. Mol. Liq. 371 (2023) 121024.

[60] Y. Zhang, Y. Xie, J. Li, T. Bai, J. Wang, Photocatalytic activity and adsorption performance of p-CuBi 2 O 4/n-TiO 2 p–n heterojunction composites prepared by in situ sol–gel coating method, J. Sol-Gel Sci. Technol. 71 (2014) 38–42.

[61] A. Huízar-Félix, T. Hernández, S. De la Parra, J. Ibarra, B. Kharisov, Sol–gel based Pechini method synthesis and characterization of Sm1− xCaxFeO3 perovskite $0.1 \leq x \leq 0.5$, Powder Technol. 229 (2012) 290–293.

[62] Z. Li, M. Chen, Q. Zhang, D. Tao, Mechanochemical synthesis of a Z-scheme Bi2WO6/CuBi2O4 heterojunction and its visible-light photocatalytic degradation of ciprofloxacin, J. Alloys Compd. 845 (2020) 156291.

[63] A. Kumar, S. Dutta, S. Kim, T. Kwon, S.S. Patil, N. Kumari, S. Jeevanandham, I. S. Lee, Solid-state reaction synthesis of nanoscale materials: strategies and applications, Chem. Rev. 122 (15) (2022) 12748–12863.

[64] J. Peng, Y. Gao, H. Zhang, Z. Liu, W. Zhang, L. Li, Y. Qiao, W. Yang, J. Wang, S. Dou, Ball milling solid-state synthesis of highly crystalline Prussian blue analogue Na2− xMnFe (CN) 6 cathodes for all-climate sodium-ion batteries, Angew. Chem. 134 (32) (2022) e202205867.

[65] L. Wei, C. Shifu, Z. Huaye, Y. Xiaoling, Preparation, characterisation of p–n heterojunction photocatalyst CuBi2O4/Bi2WO6 and its photocatalytic activities, J. Exp. Nanosci. 6 (2) (2011) 102–120.

[66] Y. Deng, Y. Chen, B. Chen, J. Ma, Preparation, characterization and photocatalytic activity of CuBi2O4/NaTaO3 coupled photocatalysts, J. Alloys Compd. 559 (2013) 116–122.

[67] M. Chen, Q. Yang, L. Li, M. Liu, P. Xiao, M. Zhang, Solid-state synthesis of CuBi2O4/MWCNT composites with enhanced photocatalytic activity under visible light irradiation, Mater. Lett. 171 (2016) 255–258.

[68] A. Elaziouti, N. Laouedj, A. Bekka, R.-N. Vannier, Preparation and characterization of p–n heterojunction CuBi2O4/CeO2 and its photocatalytic activities under UVA light irradiation, J. King Saud Univ. Sci. 27 (2) (2015) 120–135.

[69] X. Shen, Z. Zhu, H. Zhang, G. Di, Y. Qiu, D. Yin, Novel sphere-like copper bismuth oxide fabricated via ethylene glycol-introduced solvothermal method with improved adsorptive and photocatalytic performance in sulfamethazine removal, Environ. Sci. Pollut. Res. 29 (31) (2022) 47159–47173.

[70] L. Kumari, W. Li, J. Huang, P.P. Provencio, Solvothermal synthesis, structure and optical property of nanosized CoSb 3 skutterudite, Nanoscale Res. Lett. 5 (2010) 1698–1705.

[71] F. Zhang, Y. Sun, M. Li, Q. Wang, W. Song, J. Ma, J. Hou, Solvothermal preparation of hydrangea-like CuBi2O4 twining TiO2 NTAs with enhanced photoelectrocatalytic dye degradation and hydrogen generation, Colloids Surf. A Physicochem. Eng. Asp. 667 (2023) 131389.

[72] T. Ma, H. Long, Z. Shi, Z. Lang, M. Zhao, S. Zhang, C. Lei, Efficient photocatalytic degradation of TC under visible light with three-dimensional flower shaped N doped BiOBr/CuBi2O4, Opt. Mater. 143 (2023) 114175.

[73] A.C. Nogueira, L.E. Gomes, J.A. Ferencz, J.E. Rodrigues, R.V. Goncalves, H. Wender, Improved visible light photoactivity of CuBi2O4/CuO heterojunctions for photodegradation of methylene blue and metronidazole, J. Phys. Chem. C 123 (42) (2019) 25680–25690.

[74] J. Mi, X. Zhao, T. Zhu, J. Tu, G. Cao, Solvothermal synthesis and electrical transport properties of skutterudite CoSb3, J. Alloys Compd. 417 (1–2) (2006) 269–272.

[75] A. Muthukrishnaraj, S. Vadivel, I.M. Joni, N. Balasubramanian, Development of reduced graphene oxide/CuBi2O4 hybrid for enhanced photocatalytic behavior under visible light irradiation, Ceram. Int. 41 (5) (2015) 6164–6168.

[76] G. Demazeau, Solvothermal processes: definition, key factors governing the involved chemical reactions and new trends, Zeitschrift für Naturforschung B 65 (8) (2010) 999–1006.

[77] X. Yuan, D. Shen, Q. Zhang, H. Zou, Z. Liu, F. Peng, Z-scheme Bi2WO6/CuBi2O4 heterojunction mediated by interfacial electric field for efficient visible-light photocatalytic degradation of tetracycline, Chem. Eng. J. 369 (2019) 292–301.

[78] J. Hou, Y. Xie, Y. Sun, Y. Kuang, Z. Jiao, Q. Wang, Construction of a double Z-scheme Bi2O3–CuBi2O4–CuO composite photocatalyst for the enhanced photocatalytic activity, Ceram. Int. 48 (14) (2022) 20648–20657.

[79] C.G. Bruziquesi, M.C. Stolzemburg, R.R. de Souza, M. Rodriguez, M.L. Rocco, P. E. Salomão, A.E. Nogueira, Z.E. López-Cabaña, M.C. Pereira, A.C. Silva, Cobalt as a sacrificial metal to increase the photoelectrochemical stability of CuBi2O4 films for water splitting, Int. J. Hydrogen Energy 48 (9) (2023) 3456–3465.

[80] F. Wang, A. Chemseddine, F.F. Abdi, R. van de Krol, S.P. Berglund, Spray pyrolysis of CuBi 2 O 4 photocathodes: improved solution chemistry for highly homogeneous thin films, J. Mater. Chem. A 5 (25) (2017) 12838–12847.

[81] W. Shi, J.-C. Wang, X. Guo, H.-L. Tian, W. Zhang, H. Gao, H. Han, R. Li, Y. Hou, Ultra-fast construction of CuBi2O4 films supported Bi2O3 with dominant (0 2 0) facets for efficient CO2 photoreduction in water vapor, J. Alloys Compd. 890 (2022) 161919.

[82] Y. Wang, J. Hu, S. Liu, D. Zhu, B. Zhao, A. Song, Fast solvent evaporation of phase pure CuBi2O4 photocathodes for photoelectrocatalytic water splitting, J. Electroanal. Chem. 944 (2023) 117639.

[83] F. Wang, W. Septina, A. Chemseddine, F.F. Abdi, D. Friedrich, P. Bogdanoff, R. van de Krol, S.D. Tilley, S.P. Berglund, Gradient self-doped CuBi2O4 with highly improved charge separation efficiency, J. Am. Chem. Soc. 139 (42) (2017) 15094–15103.

[84] N.A. Shepelin, Z.P. Tehrani, N. Ohannessian, C.W. Schneider, D. Pergolesi, T. Lippert, A practical guide to pulsed laser deposition, Chem. Soc. Rev. 52 (2023) 2294.

[85] J. Woo, J. Lee, J. Jun, S. Kim, Y. Jung, I. Oh, S. Lee, Generation of stable photovoltage in nonstoichiometric CuBi 2 O 4 thin-film photocathodes, Int. J. Energy Res. 2023 (2023).

[86] R. Gottesman, A. Song, I. Levine, M. Krause, A.N. Islam, D. Abou-Ras, T. Dittrich, R. van de Krol, A. Chemseddine, Pure CuBi2O4 photoelectrodes with increased stability by rapid thermal processing of Bi2O3/CuO grown by pulsed laser deposition, Adv. Funct. Mater. 30 (21) (2020) 1910832.

[87] J. Lee, H. Yoon, S. Kim, S. Seo, J. Song, B.-U. Choi, S.Y. Choi, H. Park, S. Ryu, J. Oh, Long-term stabilized high-density CuBi 2 O 4/NiO heterostructure thin film photocathode grown by pulsed laser deposition, Chem. Commun. 55 (83) (2019) 12447–12450.

[88] J. Lee, H. Yoon, K.S. Choi, S. Kim, S. Seo, J. Song, B.U. Choi, J. Ryu, S. Ryu, J. Oh, Template engineering of CuBi2O4 single-crystal thin film photocathodes, Small 16 (39) (2020) 2002429.

[89] X. Zhu, Z. Guan, P. Wang, Q. Zhang, Y. Dai, B. Huang, Amorphous TiO2-modified CuBi2O4 photocathode with enhanced photoelectrochemical hydrogen production activity, Chin. J. Catal. 39 (10) (2018) 1704–1710.

[90] L. Zhao, X. Wang, Z. Liu, Efficient photoelectrochemical performances of the novel honeycomb network-like CuBi 2 O 4 films, Appl. Phys. A 124 (2018) 1–7.

[91] X. Lu, J. Xie, L. Wang, J. Ren, S. Yang, Q. Yang, S. Wang, C. Huang, P. Yang, CuBi2O4/CuO heterojunction coated with electrodeposited ZnO overlayer for stable solar hydrogen evolution, J. Electroanal. Chem. 937 (2023) 117421.

[92] Y. Nakabayashi, M. Nishikawa, N. Saito, Relationship between the morphology for the photo-electrode of copper bismuth oxide and the photo-electrochemical activity related to water reduction, J. Chem. Sci. 133 (2021) 1–10.

[93] Y. Nakabayashi, M. Nishikawa, Y. Nosaka, Fabrication of CuBi2O4 photocathode through novel anodic electrodeposition for solar hydrogen production, Electrochim. Acta 125 (2014) 191–198.

[94] N.T. Hahn, V.C. Holmberg, B.A. Korgel, C.B. Mullins, Electrochemical synthesis and characterization of p-CuBi2O4 thin film photocathodes, J. Phys. Chem. C 116 (10) (2012) 6459–6466.

[95] S. Liu, J. Zhou, Y. Lu, J. Su, Pulsed laser/electrodeposited CuBi2O4/BiVO4 pn heterojunction for solar water splitting, Sol. Energy Mater. Sol. Cells 180 (2018) 123–129.

[96] X. Yang, D. Wang, Photocatalysis: from fundamental principles to materials and applications, ACS Appl. Energy Mater. 1 (12) (2018) 6657–6693.

[97] S. Zhu, D. Wang, Photocatalysis: basic principles, diverse forms of implementations and emerging scientific opportunities, Adv. Energy Mater. 7 (23) (2017) 1700841.

[98] J. Low, J. Yu, M. Jaroniec, S. Wageh, A.A. Al-Ghamdi, Heterojunction photocatalysts, Adv. Mater. 29 (20) (2017) 1601694.

[99] S. Bagheri, A. TermehYousefi, T.-O. Do, Photocatalytic pathway toward degradation of environmental pharmaceutical pollutants: structure, kinetics and mechanism approach, Cat. Sci. Technol. 7 (20) (2017) 4548–4569.

[100] S. Banerjee, S.C. Pillai, P. Falaras, K.E. O'shea, J.A. Byrne, D.D. Dionysiou, New insights into the mechanism of visible light photocatalysis, J. Phys. Chem. Lett. 5 (15) (2014) 2543–2554.

[101] L. Che, J. Pan, K. Cai, Y. Cong, S.-W. Lv, The construction of p-n heterojunction for enhancing photocatalytic performance in environmental application: a review, Sep. Purif. Technol. 315 (2023) 123708.

[102] W. Tahir, T.-Y. Cheang, J.-H. Li, C. Ling, X.-J. Lu, I. Ullah, G. Wang, A.-W. Xu, Interfacial Ti≡ N bonding of a g-C3N4/TiH1. 92 type-II heterojunction photocatalyst significantly enhanced photocatalytic hydrogen evolution from water splitting, Catal. Sci. Technol. 12 (6) (2022) 2023–2029.

[103] J. Li, H. Yuan, W. Zhang, B. Jin, Q. Feng, J. Huang, Z. Jiao, Advances in Z-scheme semiconductor photocatalysts for the photoelectrochemical applications: a review, Carbon Energy 4 (3) (2022) 294–331.

[104] J. Fu, Q. Xu, J. Low, C. Jiang, J. Yu, Ultrathin 2D/2D WO3/g-C3N4 step-scheme H2-production photocatalyst, Appl. Catal. Environ. 243 (2019) 556–565.

[105] D. Liu, D. Chen, N. Li, Q. Xu, H. Li, J. He, J. Lu, ZIF-67-derived 3D hollow mesoporous crystalline Co3O4 wrapped by 2D g-C3N4 nanosheets for photocatalytic removal of nitric oxide, Small 15 (31) (2019) 1902291.

[106] K. Priya, G.K. Rao, G. Sanjeev, The fabrication and characterization of thermal evaporated n-ZnS/p-Si heterojunction and ZnS-Au Schottky photodiodes, Opt. Laser Technol. 157 (2023) 108657.

[107] A. Behera, D. Kandi, S. Martha, K. Parida, Constructive interfacial charge carrier separation of a p-CaFe2O4@ n-ZnFe2O4 heterojunction architect photocatalyst toward photodegradation of antibiotics, Inorg. Chem. 58 (24) (2019) 16592–16608.

[108] M. Li, Y. Gong, Y. Wang, T. He, Probing interfacial charge transfer in heterojunctions for photocatalysis, Phys. Chem. Chem. Phys. 24 (33) (2022) 19659–19672.

[109] R. Marschall, Semiconductor composites: strategies for enhancing charge carrier separation to improve photocatalytic activity, Adv. Funct. Mater. 24 (17) (2014) 2421–2440.

[110] Z. Li, R. Zheng, S. Dai, T. Zhao, M. Chen, Q. Zhang, In-situ mechanochemical fabrication of p-n Bi2MoO6/CuBi2O4 heterojunctions with efficient visible light photocatalytic performance, J. Alloys Compd. 882 (2021) 160681.

[111] K.X. Song, C. Zhang, Y. Zhang, G.L. Yu, M.J. Zhang, Y.Y. Zhang, L. Qiao, M.S. Liu, N. Yin, Y. Zhao, Y.N. Tao, Efficient tetracycline degradation under visible light irradiation using CuBi₂O₄/ZnFe₂O₄ type II heterojunction photocatalyst based on two spinel oxides, J. Photochem. Photobiol. A Chem. 433 (2022).

[112] A.C. Nogueira, L.E. Gomes, J.A.P. Ferencz, J. Rodrigues, R.V. Gonçalves, H. Wender, Improved visible light photoactivity of CuBi₂O₄/CuO heterojunctions for photodegradation of methylene blue and metronidazole, J. Phys. Chem. C 123 (42) (2019) 25680–25690.

[113] F. Guo, W.L. Shi, H.B. Wang, M.M. Han, W.S. Guan, H. Huang, Y. Liu, Z.H. Kang, Study on highly enhanced photocatalytic tetracycline degradation of type II AgI/CuBi₂O₄ and Z-scheme AgBr/CuBi₂O₄ heterojunction photocatalysts, J. Hazard. Mater. 349 (2018) 111–118.

[114] Z.W. Wu, Z.M. Zhang, M.D. Sun, B. Tan, B. Liu, W.H. Han, E.Q. Xie, Y.T. Li, Self-powered photodetector based on p-type CuBi₂O₄ with fermi level engineering, Adv. Mater. Interfaces 8 (24) (2021).

[115] L. Schumacher, R. Marschall, Recent advances in semiconductor heterojunctions and Z-schemes for photocatalytic hydrogen generation, Top. Curr. Chem. 380 (6) (2022) 53.

[116] S. Bai, J. Jiang, Q. Zhang, Y. Xiong, Steering charge kinetics in photocatalysis: intersection of materials syntheses, characterization techniques and theoretical simulations, Chem. Soc. Rev. 44 (10) (2015) 2893–2939.

[117] V. Hasija, A. Kumar, A. Sudhaik, P. Raizada, P. Singh, Q. Van Le, T.T. Le, V.-H. Nguyen, Step-scheme heterojunction photocatalysts for solar energy, water splitting, CO2 conversion, and bacterial inactivation: a review, Environ. Chem. Lett. 19 (4) (2021) 2941–2966.

[118] M.J. Molaei, Principles, mechanism, and identification of S-scheme heterojunction for photocatalysis: a critical review, J. Am. Ceram. Soc. 107 (2024) 5695.

[119] J. Luo, X. Zhou, F. Yang, X. Ning, L. Zhan, Z. Wu, X. Zhou, Generating a captivating S-scheme CuBi2O4/CoV2O6 heterojunction with boosted charge spatial separation for efficiently removing tetracycline antibiotic from wastewater, J. Clean. Prod. 357 (2022) 131992.

[120] X.C. Dou, Y.G. Chen, H.F. Shi, $CuBi_2O_4$/BiOBr composites promoted PMS activation for the degradation of tetracycline: S-scheme mechanism boosted Cu^{2+}/Cu^{+} cycle, Chem. Eng. J. (2022) 431.

[121] J.C. Wang, H.R. Ma, W.A. Shi, W. Li, Z.G. Zhang, Y.X. Hou, W.Q. Zhang, J. Chen, Designed synthesized step-scheme heterojunction of Bi_2WO_6 nanosheet supported on $CuBi_2O_4$ nanorod with remarkable photo-assisted gas sensing for N-butyl alcohol, J. Environ. Chem. Eng. 12 (3) (2024).

[122] J.C. Wang, B.B. Wang, W.N. Shi, X. Qiao, X.X. Yang, L.F. Zhang, W.Q. Zhang, R. L. Li, Y.X. Hou, Natural-sunlight-driven synchronous degradation of 4-nitrphenol and rhodamine B over S-scheme heterojunction of α-Fe_2O_3 nanoparticles decorated $CuBi_2O_4$ rods, J. Environ. Chem. Eng. 10 (6) (2022).

[123] U. Ghosh, A. Pal, Graphitic carbon nitride based Z scheme photocatalysts: design considerations, synthesis, characterization and applications, J. Ind. Eng. Chem. 79 (2019) 383–408.

[124] Y. Sasaki, A. Iwase, H. Kato, A. Kudo, The effect of co-catalyst for Z-scheme photocatalysis systems with an Fe^{3+}/Fe^{2+} electron mediator on overall water splitting under visible light irradiation, J. Catal. 259 (1) (2008) 133–137.

[125] Y. Iwase, O. Tomita, M. Higashi, A. Nakada, R. Abe, Effective strategy for enhancing Z-scheme water splitting with the IO^{3-}/I^{-} redox mediator by using a visible light responsive TaON photocatalyst co-loaded with independently optimized two different cocatalysts, Sustainable Energy Fuels 3 (6) (2019) 1501–1508.

[126] Q. Xiang, J. Yu, M. Jaroniec, Graphene-based semiconductor photocatalysts, Chem. Soc. Rev. 41 (2) (2012) 782–796.

[127] M. Ghobadifard, P.V. Radovanovic, S. Mohebbi, Novel CoFe2O4/CuBi2O4 heterojunction p–n semiconductor as visible-light-driven nanophotocatalyst for C (OH)–H bond activation, Appl. Organomet. Chem. 36 (4) (2022) e6612.

[128] D. Sun, Y. Chen, X. Yu, Y. Yin, G. Tian, Novel defect-transit dual Z-scheme heterojunction: sulfur-doped carbon nitride nanotubes loaded with bismuth oxide and bismuth sulfide for efficient photocatalytic amine oxidation, J. Colloid Interface Sci. 674 (2024) 225.

[129] K. Zhou, Y. Liu, J. Hao, One-pot hydrothermal synthesis of dual Z-scheme BiOBr/g-C3N4/Bi2WO6 and photocatalytic degradation of tetracycline under visible light, Mater. Lett. 281 (2020) 128463.

[130] Z. Li, Y. Zhao, Q. Guan, Q. Liu, S. Khan, L. Zhang, X. Wang, L. Chen, X. Yang, M. Huo, Novel direct dual Z-scheme AgBr (Ag)/MIL-101 (Cr)/CuFe2O4 for efficient conversion of nitrate to nitrogen, Appl. Surf. Sci. 508 (2020) 145225.

[131] Y. Deng, L. Tang, G. Zeng, C. Feng, H. Dong, J. Wang, H. Feng, Y. Liu, Y. Zhou, Y. Pang, Plasmonic resonance excited dual Z-scheme BiVO 4/Ag/Cu 2 O nanocomposite: synthesis and mechanism for enhanced photocatalytic performance in recalcitrant antibiotic degradation, Environ. Sci. Nano 4 (7) (2017) 1494–1511.

[132] R. Kumar, A. Sudhaik, A.A.P. Khan, P. Raizada, A.M. Asiri, S. Mohapatra, S. Thakur, V.K. Thakur, P. Singh, Current status on designing of dual Z-scheme photocatalysts for energy and environmental applications, J. Ind. Eng. Chem. 106 (2022) 340–355.

[133] P.J. Mafa, M.E. Malefane, A.O. Idris, B.B. Mamba, D. Liu, J. Gui, A.T. Kuvarega, Cobalt oxide/copper bismuth oxide/samarium vanadate (Co3O4/CuBi2O4/SmVO4) dual Z-scheme heterostructured photocatalyst with high charge-transfer efficiency: enhanced carbamazepine degradation under visible light irradiation, J. Colloid Interface Sci. 603 (2021) 666–684.

[134] A. Di Bartolomeo, Graphene Schottky diodes: an experimental review of the rectifying graphene/semiconductor heterojunction, Phys. Rep. 606 (2016) 1–58.

[135] M.R. Khan, T.W. Chuan, A. Yousuf, M.N.K. Chowdhury, C.K. Cheng, Schottky barrier and surface plasmonic resonance phenomena towards the photocatalytic reaction: study of their mechanisms to enhance photocatalytic activity, Cat. Sci. Technol. 5 (5) (2015) 2522–2531.

[136] M. Rycenga, C.M. Cobley, J. Zeng, W. Li, C.H. Moran, Q. Zhang, D. Qin, Y. Xia, Controlling the synthesis and assembly of silver nanostructures for plasmonic applications, Chem. Rev. 111 (6) (2011) 3669–3712.

[137] Y. Xia, Y. Xiong, B. Lim, S.E. Skrabalak, Cover picture: shape-controlled synthesis of metal nanocrystals: simple chemistry meets complex physics? (Angew. Chem. Int. Ed. 1/2009), Angew. Chem. Int. Ed. 48 (1) (2009) 1.

[138] D.B. Ingram, P. Christopher, J.L. Bauer, S. Linic, Predictive model for the design of plasmonic metal/semiconductor composite photocatalysts, ACS Catal. 1 (10) (2011) 1441–1447.

[139] P. Kumari, N. Bahadur, L. Kong, L.A. O'Dell, A. Merenda, L.F. Dumée, Engineering Schottky-like and heterojunction materials for enhanced photocatalysis performance – a review, Mater. Adv. 3 (5) (2022) 2309–2323.

[140] W. Shi, M. Li, H. Ren, F. Guo, X. Huang, Y. Shi, Y. Tang, Construction of a 0D/1D composite based on Au nanoparticles/CuBi2O4 microrods for efficient visible-light-driven photocatalytic activity, Beilstein J. Nanotechnol. 10 (2019) 1360–1367.

[141] A.M. Djaballah, R. Bagtache, M. Benlembarek, M. Trari, Synthesis and characterization of Pt/CuBi2O4. Application to photocatalytic H2 evolution under visible light, J. Photochem. Photobiol. A Chem. 447 (2024) 115186.

[142] Z.Y. Zhang, X.L. Hao, S. Hao, J.Y. Li, Preparation of Pd@CuBi₂O₄ photocatalysts and their performance for selective oxidation of benzyl alcohol under visible light illumination, Mater. Sci. Semicond. Process. 142 (2022).

[143] V. Dutta, S. Sonu, P. Raizada, V.K. Thakur, T. Ahamad, S. Thakur, P. Kumar Verma, H.H.P. Quang, V.-H. Nguyen, P. Singh, Prism-like integrated Bi2WO6 with Ag-CuBi2O4 on carbon nanotubes (CNTs) as an efficient and robust S-scheme interfacial charge transfer photocatalyst for the removal of organic pollutants from wastewater, Environ. Sci. Pollut. Res. 30 (2022) 124530.

[144] L. Zhang, Q. Shen, F. Huang, L. Jiang, J. Liu, J. Sheng, Y. Li, H. Yang, Electrospinning directly synthesis of 0D/1D CuBi2O4@WO3 nanofiber photocatalyst with S-scheme heterojunction, Appl. Surf. Sci. 608 (2023) 155064.

[145] I. Ani, U. Akpan, M. Olutoye, B. Hameed, Photocatalytic degradation of pollutants in petroleum refinery wastewater by TiO2-and ZnO-based photocatalysts: recent development, J. Clean. Prod. 205 (2018) 930–954.

[146] G. Li, K. Wong, X. Zhang, C. Hu, C.Y. Jimmy, R. Chan, P. Wong, Degradation of acid orange 7 using magnetic AgBr under visible light: the roles of oxidizing species, Chemosphere 76 (9) (2009) 1185–1191.

[147] M. Sabri, A. Habibi-Yangjeh, S. Ghosh, Novel ZnO/CuBi2O4 heterostructures for persulfate-assisted photocatalytic degradation of dye contaminants under visible light, J. Photochem. Photobiol. A Chem. 391 (2020) 112397.

[148] H. Lahmar, M. Benamira, F.Z. Akika, M. Trari, Reduction' of chromium (VI) on the hetero-system CuBi₂O₄/TiO₂ under solar light, J. Phys. Chem. Solid 110 (2017) 254–259.

[149] P. Thammaacheep, K. Chansaenpak, P. Jannoey, W. Khanitchaidecha, A. Nakaruk, D. Channei, Modification of Co₃O₄/CuBi₂O₄ composite for photocatalytic degradation of methylene blue dye, Desalin. Water Treat. 267 (2022) 283–292.

[150] E. Abdelkader, L. Nadjia, B. Ahmed, Synthesis, characterization and UV-A light photocatalytic activity of 20 wt%SrO-CuBi₂O₄ composite, Appl. Surf. Sci. 258 (12) (2012) 5010–5024.

[151] J.-C. Wang, B. Wang, W. Shi, X. Qiao, X. Yang, L. Zhang, W. Zhang, R. Li, Y. Hou, Natural-sunlight-driven synchronous degradation of 4-nitrphenol and rhodamine B over S-scheme heterojunction of α-Fe2O3 nanoparticles decorated CuBi2O4 rods, J. Environ. Chem. Eng. 10 (6) (2022) 108565.

[152] J. Zhu, M. Liao, C. Zhao, M. Liu, A. Han, C. Zhu, Y. Sun, M. Zhao, S. Ye, H. Cao, A comprehensive review on semiconductor-based photocatalysts toward the degradation of persistent pesticides, Nano Res. 16 (5) (2023) 6402–6443.

[153] R. Zhou, D. Zhang, P. Wang, Y. Huang, Regulation of excitons dissociation in AgI/Bi3O4Br for advanced reactive oxygen species generation towards photodegradation, Appl. Catal. Environ. 285 (2021) 119820.

[154] Y. Zhou, H. Deng, Z. Li, Y. Wang, T. Ma, Construction of CuBi2O4/BiOBr/biochar Z-scheme heterojunction for degradation of gaseous benzene under visible light, Catal. Lett. 153 (8) (2023) 2319–2330.

[155] S. Fu, H. Zhu, Q. Huang, X. Liu, X. Zhang, J. Zhou, Construction of hierarchical CuBi2O4/Bi/BiOBr ternary heterojunction with Z-scheme mechanism for enhanced broad-spectrum photocatalytic activity, J. Alloys Compd. 878 (2021) 160372.

[156] J. Tian, L. Wei, J. Hu, J. Lu, Boosting reactive oxygen species generation over Bi3O4Br/CuBi2O4 by activating peroxymonosulfate under visible light irradiation, Sep. Purif. Technol. 289 (2022) 120794.

[157] J. Qiu, Y. Wang, X. Liu, One-pot hydrothermal synthesis of CuBi2O4/BiOCl p–n heterojunction with enhanced photocatalytic performance for the degradation of tetracycline hydrochloride under visible light irradiation, New J. Chem. 46 (6) (2022) 2898–2907.

[158] D. Chen, Q. Wang, R. Wang, G. Shen, Ternary oxide nanostructured materials for supercapacitors: a review, J. Mater. Chem. A 3 (19) (2015) 10158–10173.

[159] F.F. Abdi, S.P. Berglund, Recent developments in complex metal oxide photoelectrodes, J. Phys. D Appl. Phys. 50 (19) (2017) 193002.

[160] X.J. Yuan, D.Y. Shen, Q. Zhang, H.B. Zou, Z.L. Liu, F. Peng, Z-scheme Bi₂WO₆/CuBi₂O₄ heterojunction mediated by interfacial electric field for efficient visible-light photocatalytic degradation of tetracycline, Chem. Eng. J. 369 (2019) 292–301.

[161] Y. Hu, H. Hao, Y. Zhao, J. Min, Q. Huang, J. Zhong, G. Zhang, J. Bi, S. Yan, H. Hou, Construction of pyroelectrically-driven BiFeO3@CuBi2O4 nanofiber composite catalyst for enhanced pyrocatalytic activities under room-temperature cold and hot cycles, Surf. Interfaces 33 (2022) 102191.

[162] H. Ramezanalizadeh, E. Rafiee, Design, fabrication, electro- and photoelectrochemical investigations of novel CoTiO₃/CuBi₂O₄ heterojunction semiconductor: An efficient photocatalyst for the degradation of DR16 dye, Mater. Sci. Semicond. Process. (2020) 113.

[163] R. Huang, X. Liu, X. Yang, Z. Rao, W. Cai, Z. Wang, R. Gao, G. Chen, X. Deng, X. Lei, C. Fu, Piezo-phototronic coupling effect in CuBi2O4/AgNbO3 Z-scheme heterojunction for high-efficiency decomposition of organic dye, ACS Appl. Electron. Mater. 5 (11) (2023) 6197–6211.

[164] Z. Yu, Y. Zhou, H. Zhang, M. Zhang, R. Zhang, H. Yin, J. Wang, One-pot hydrothermal preparation of rich-oxygen vacant Bi2SiO5/CuBi2O4 Z-scheme heterojunction for visible light-driven photocatalytic removal of antibiotic-resistant bacteria, Chem. Eng. J. 478 (2023) 147353.

[165] L. Dou, J. Zhong, J. Li, J. Luo, Y. Zeng, Fabrication of Bi2SiO5 hierarchical microspheres with an efficient photocatalytic performance for rhodamine B and phenol removal, Mater. Res. Bull. 116 (2019) 50–58.

[166] C.-T. Yang, W.W. Lee, H.-P. Lin, Y.-M. Dai, H.-T. Chi, C.-C. Chen, A novel heterojunction photocatalyst, Bi 2 SiO 5/gC 3 N 4: synthesis, characterization, photocatalytic activity, and mechanism, RSC Adv. 6 (47) (2016) 40664–40675.

[167] R.A. Mahmud, A.N. Shafawi, K. Ahmed Ali, L.K. Putri, N.I. Md Rosli, A. R. Mohamed, Graphene nanoplatelets with low defect density as a synergetic adsorbent and electron sink for ZnO in the photocatalytic degradation of methylene blue under UV–vis irradiation, Mater. Res. Bull. 128 (2020) 110876.

[168] T.-F. Yeh, J. Cihlář, C.-Y. Chang, C. Cheng, H. Teng, Roles of graphene oxide in photocatalytic water splitting, Mater. Today 16 (3) (2013) 78–84.

[169] L.P. Bakos, L. Sárvári, K. László, J. Mizsei, Z. Kónya, G. Halasi, K. Hernádi, A. Szabó, D. Berkesi, I. Bakos, I.M. Szilágyi, Electric and photocatalytic properties of graphene oxide depending on the degree of its reduction, Nanomaterials (Basel) 10 (11) (2020).
[170] H. Chen, L. Wang, Nanostructure sensitization of transition metal oxides for visible-light photocatalysis, Beilstein J. Nanotechnol. 5 (2014) 696–710.
[171] P. Annamalai, D. Thangavelu, M. Ramadoss, S. Subramani, S.P. Muthu, R. Perumalsamy, S. Ranganathan, V. Hector, Electrochemical sensing of tyrosine and removal of toxic dye using self-assembled three-dimensional CuBi2O4/rGO microsphere composite, Colloid Interface Sci. Commun. 45 (2021) 100523.
[172] V. Dutta, P. Sonu, P.K. Raizada, T. Verma, S. Ahamad, C.M. Thakur, P. Singh Hussain, Constructing carbon nanotubes@CuBi2O4/AgBiO3 all solid-state mediated Z-scheme photocatalyst with enhanced photocatalytic activity, Mater. Lett. 320 (2022) 132374.
[173] M. Mousavi, M. Hamzehloo, J.B. Ghasemi, Deposited CuBi 2 O 4 and Bi 3 ClO 4 nanoparticles on gC 3 N 4 nanosheet: a promising visible light-induced photocatalyst toward the removal of tetracycline hydrochloride and rhodamine B, J. Mater. Sci. 55 (2020) 7775–7791.
[174] N. Ahmad, J. Anae, M.Z. Khan, S. Sabir, P. Campo, F. Coulon, A novel CuBi2O4/polyaniline composite as an efficient photocatalyst for ammonia degradation, Heliyon 8 (8) (2022).
[175] A. Song, P. Plate, A. Chemseddine, F. Wang, F.F. Abdi, M. Wollgarten, R. van de Krol, S.P. Berglund, Cu: NiO as a hole-selective back contact to improve the photoelectrochemical performance of CuBi 2 O 4 thin film photocathodes, J. Mater. Chem. A 7 (15) (2019) 9183–9194.
[176] J.S. Compton, C.A. Peterson, D. Dervishogullari, L.R. Sharpe, Spray pyrolysis as a combinatorial method for the generation of photocatalyst libraries, ACS Comb. Sci. 21 (6) (2019) 489–499.
[177] F. Cai, T. Zhang, Q. Liu, P. Guo, Y. Lei, Y. Wang, F. Wang, One step synthesis of tetragonal-CuBi2O4/amorphous-bifeo3 heterojunction with improved charge separation and enhanced photocatalytic properties, Nanomaterials 10 (8) (2020) 1514.
[178] Z. Wang, Q. Wu, J. Wang, Y. Yu, Surface modification by ligand growth strategy for dense copper bismuth film as photocathode to enhance hydrogen production activity, Front. Energy (2023) 1–12.
[179] L. Wang, G. Yang, D. Wang, C. Lu, W. Guan, Y. Li, J. Deng, J. Crittenden, Fabrication of the flower-flake-like CuBi2O4/Bi2WO6 heterostructure as efficient visible-light driven photocatalysts: performance, kinetics and mechanism insight, Appl. Surf. Sci. 495 (2019) 143521.
[180] T.O. Ajiboye, D.C. Onwudiwe, Bismuth sulfide based compounds: properties, synthesis and applications, Results Chem. 3 (2021) 100151.
[181] M. Gopannagari, K.A.J. Reddy, S. Inae, H.S. Bae, J. Lee, T.G. Woo, A.P. Rangappa, D.P. Kumar, D.A. Reddy, T.K. Kim, High-performance silver-doped porous CuBi2O4 photocathode integrated with NiO hole-selective layer for improved photoelectrochemical water splitting, Adv. Sustain. Syst. 7 (8) (2023) 2300085.
[182] A.C. Nogueira, L.E. Gomes, J.A.P. Ferencz, J.E.F.S. Rodrigues, R.V. Gonçalves, H. Wender, Improved visible light photoactivity of CuBi2O4/CuO heterojunctions for photodegradation of methylene blue and metronidazole, J. Phys. Chem. C 123 (42) (2019) 25680–25690.
[183] D. Majhi, A. Kumar Mishra, K. Das, R. Bariki, B.G. Mishra, Plasmonic Ag nanoparticle decorated Bi2O3/CuBi2O4 photocatalyst for expeditious degradation of 17α-ethinylestradiol and Cr(VI) reduction: insight into electron transfer mechanism and enhanced photocatalytic activity, Chem. Eng. J. 413 (2021) 127506.
[184] C. Fang, H. Su, M. Hu, Z. Jiang, L. Xu, C. Liu, Construction and performance of a novel CuBi2O4/In2O3 Z-scheme heterojunction photocatalyst, Mater. Sci. Semicond. Process. 160 (2023) 107464.
[185] M. Azimifar, M. Ghorbani, M. Peyravi, Fabrication and evaluation of a photocatalytic membrane based on Sb2O3/CBO composite for improvement of dye removal efficiency, J. Mol. Struct. 1270 (2022) 133957.
[186] H. Lahmar, M. Benamira, F.Z. Akika, M. Trari, Reduction of chromium (VI) on the hetero-system CuBi2O4/TiO2 under solar light, J. Phys. Chem. Solid 110 (2017) 254–259.
[187] L. Wang, T. Huang, G. Yang, C. Lu, F. Dong, Y. Li, W. Guan, The precursor-guided hydrothermal synthesis of CuBi2O4/WO3 heterostructure with enhanced photoactivity under simulated solar light irradiation and mechanism insight, J. Hazard. Mater. 381 (2020) 120956.
[188] F. Guo, M.Y. Li, H.J. Renb, X.L. Huang, W.X. Hou, C. Wang, W.L. Shi, C.Y. Lu, Fabrication of p-n CuBi₂O₄/MoS₂ heterojunction with nanosheets-on-microrods structure for enhanced photocatalytic activity towards tetracycline degradation, Appl. Surf. Sci. 491 (2019) 88–94.
[189] X. Zhang, X. Wang, J. Chai, S. Xue, R. Wang, L. Jiang, J. Wang, Z. Zhang, D. D. Dionysiou, Construction of novel symmetric double Z-scheme BiFeO3/CuBi2O4/BaTiO3 photocatalyst with enhanced solar-light-driven photocatalytic performance for degradation of norfloxacin, Appl. Catal. Environ. 272 (2020) 119017.
[190] J. Xu, Y. Zhu, Z. Liu, X. Teng, H. Gao, Y. Zhao, M., Chen synthesis of dual Z-scheme CuBi2O4/Bi2Sn2O7/Sn3O4 photocatalysts with enhanced photocatalytic performance for the degradation of tetracycline under visible light irradiation, Catalysts (2023) 13, https://doi.org/10.3390/catal13071028.
[191] K. Dilly Rajan, P.P. Gotipamul, S. Khanna, S. Chidambaram, M. Rathinam, Piezo-photocatalytic effect of NaNbO3 interconnected nanoparticles decorated CuBi2O4 nanocuboids, Mater. Lett. 296 (2021) 129902.
[192] K. Song, C. Zhang, Y. Zhang, G. Yu, M. Zhang, Y. Zhang, L. Qiao, M. Liu, N. Yin, Y. Zhao, Y. Tao, Efficient tetracycline degradation under visible light irradiation using CuBi2O4/ZnFe2O4 type II heterojunction photocatalyst based on two spinel oxides, J. Photochem. Photobiol. A Chem. 433 (2022) 114122.